Chapter 3

Physico-Chemical Characterization

Physicochemical characterization of the prepared catalysts is usually done to ensure the purity of the systems and to get an insight to the nature of the active sites on the catalyst surface. Characterization of the prepared catalysts were done by different techniques such as X-ray diffraction analysis, energy dispersive X-ray analysis, surface area and pore volume measurements, scanning electron spectroscopy, infrared spectroscopy, thermogravimetry, UV-Vis diffuse reflectance spectroscopy and ^{1}H NMR spectroscopy. Strength and distribution of acid site were determined by three independent methods *viz.* ammonia TPD, perylene adsorption and thermodesorption of 2,6-dimethylpyridine. Cumene conversion reaction was employed to quantify the various types of acid sites on the surface of the catalysts. Acid base property of the catalysts was evaluated by cyclohexanol decomposition reaction.

3.1 INTRODUCTION

In heterogeneous catalysis, the reaction occurs at the surface. Catalysts and catalytic surfaces, hence, need to be characterized by reference to their physical properties and by their actual performance as a catalyst. The most important physical properties are those relating to the surface because catalyst performance is determined by surface parameters[1]. Atoms on surfaces are distinctly different from those in the bulk in terms of unsaturated coordination,

electronic properties and crystallographic arrangements. It is essential to know the exact structure of surface including defects as well as exact location of active sites. We present a brief discussion on characterization of surfaces of the catalysts since they are primarily responsible for catalytic activity of substances. Since solid supported catalysts and the sulfated metal oxides are well known for its surface acidity, a more detailed investigation of the acidity of the prepared systems are also discussed.

3.2 PHYSICAL CHARACTERIZATION

The catalyst systems synthesized were characterized by adopting various physical methods. The results are discussed in the following sections.

I. X-RAY DIFFRACTION ANALYSIS (XRD)

XRD profiles of titania and sulfated titania calcined at 500°C is given in figure 3.1. After calcination at 500°C, anatase appears as a crystalline phase manifested by its 101 peak (2θ = 25.5°). The anatase-rutile transformation takes place at this temperature and is confirmed by the occurrence of the 110 peak of rutile at 2θ = 27.5°). The sulfated titania possesses only diffraction lines, such as at 2θ = 25.5, 37.4, 48 and 53° simply indicating the anatase type of TiO_2. Diffraction lines for the rutile type of TiO_2 are observed at 2θ = 27, 36, 41 and 54° in the case of pure titania. The peaks corresponding to the rutile phase is completely eliminated in the case of sulfated samples. This indicates that sulfation retards the transformation from anatase to rutile in comparison with the sample without sulfation. The powder X-ray diffractograms of metal incorporated sulfated titania systems are shown in figures 3.2 and 3.3. The transition of amorphous TiO_2 to crystalline anatase TiO_2 takes place at 350 and 500°C for pure titania and sulfated titania respectively[2]. The intensity of XRD characteristic peaks of anatase TiO_2 for sulfated titania samples were lower and broader than those for the pure

titania. These observations are in support of the generally recognized viewpoint that sulfation inhibits the sintering of titania and stabilizes the surface area of sulfated titania catalyst[3].

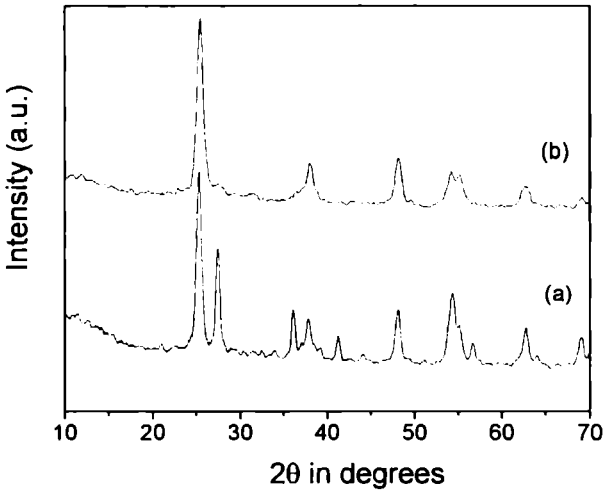

Figure 3.1 XRD profile of (a) T (b) ST

It is reported that ZrO_2 notably delay the anatase to rutile transformation, stabilizing the anatase phase[4]. In addition to stabilizing anatase TiO_2 crystallites, sulfate surface species inhibit sintering of TiO_2 crystallites leading to lower crystallites than in pure TiO_2. Low peak intensity, in the case of sulfate treated samples, indicates low crystallinity. It has been reported that the degree of crystallization of the sulfated oxides is much lower than that of the oxides without sulfation[5-7]. Dispersion of SO_4^{2-} species hinders agglomerization of the titania particles indicating delayed crystallization. The absence of any change in the peak intensity after sulfate treatment indicates that the amount of sulfate retained on the surface is insufficient to cause any change in the diffraction pattern and it is well dispersed on the surface.

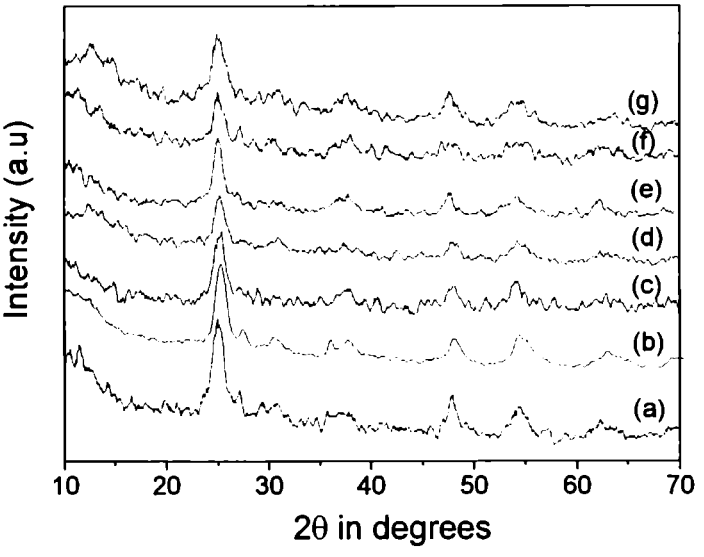

Figure 3.2:- XRD profiles of (a) STCr(3) (b) STMn(3) (c) STFe(3) (d) STCo(3) (e) STNi(3) (f) STCu(3) (f) STZn(3)

The average crystallite size is calculated using Scherrer equation[8] from the 101 reflection of anatase is given in table 3.1. The average crystallite size of titania decreases in presence of sulfate ion. The crystallite size decrease in presence of sulfate ions as SO_4^{2-} species could possibly interact with TiO_2 network and thus, hinder the growth of the particle. Even a very small amount of SO_4^{2-} species can be responsible for this effect. This type of effect is also observed in PO_4^{3-} [9,10] and WO_3[11,12]. From our earlier studies[13] it is noted that, crystallite size of titania decreases in the presence of sulfate ion, irrespective of the percentage of sulfate loading. This indicates that the crystallinity is more or less dependent on the presence of sulfate ion, but not on the percentage of sulfate loading. Among the different metal incorporated systems, chromia loaded systems show the lowest crystallite size. In the case of iron and nickel loaded samples there is an increase in the crystallite size than sulfated titania

due to the formation of bulk metal oxide rather than the dispersed form on the surface of titania. As the metal content increases the crystallite size increases.

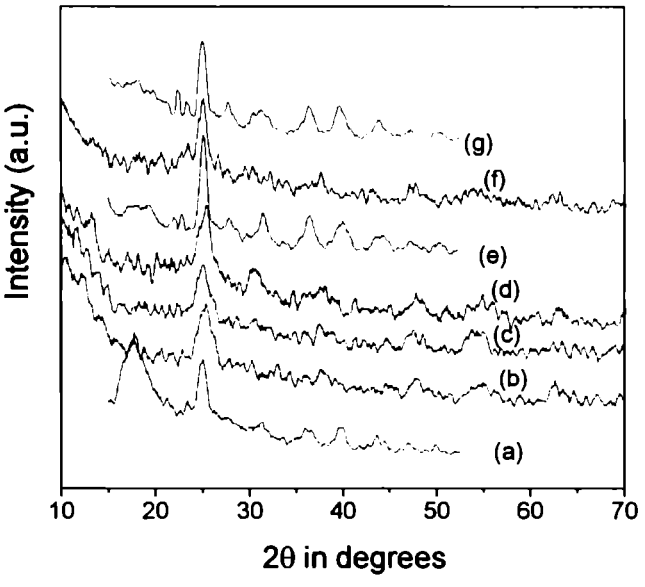

Figure 3.3 XRD profiles of (a) STCr(9) (b) STMn(9) (c) STFe(9) (d) STCo(9) (e) STNi(9) (f) STCu(9) (f) STZn(9)

Since no titanium sulfate is detected by XRD for the catalysts examined in the present study, the sulfur may exist in a form of sulfate on the surface of TiO_2. Choo *et al.*[14] reported that there was no formation of titanium sulfate for the ST calcined even at 900°C. In order to identify the state of sulfur species on the surface of TiO_2, they examined the sulfated supports by XPS and found that the sulfur compound exists in a form of sulfate (SO_4^{2-}) on the catalyst surface. The bulk structure of titania remains virtually unchanged by the incorporation of metal ions, except for a lowering in crystallinity. The absence of any characteristic peaks of the metal oxides, suggest that these oxides are present in the form of dispersed oxide species, since the total content of them is rather small and may be below the limits of detection with the XRD

technique. The bulk structure remains virtually unchanged by the incorporation of transition metals, except for a lowering in crystallinity.

II. SURFACE AREA AND PORE VOLUME MEASUREMENTS

The surface areas and pore volumes of the prepared catalysts are given in tables 3.1 and 3.2 measured using BET method by nitrogen adsorption at liquid nitrogen temperature. From the tables it is observed that pure titania has a BET surface area of 35 $m^2 g^{-1}$ and Langmuir surface area of 45 $m^2 g^{-1}$. The surface area and pore volume of the sulfated samples are invariably higher than pure titania. Superacidity is created by adsorbing sulfate ions into amorphous metal oxides followed by calcination in air to convert to the crystalline forms. Specific surface areas of the sulfated catalysts are much larger than those of the oxides without the sulfate treatment. The main reason of surface area increment is due to the retardation of crystallization of the support oxides by the sulfate groups present on the surface[15]. The lowering of degree of crystallinity, as evident from the XRD patterns, supports the increase in the surface area by sulfate treatment.

It has been noted by Ma *et al.*[16] that the crystalline grain and specific surface area of the oxide precursor exert a significant influence on the properties of the catalyst. Since sulfation of the oxide is carried out by SO_4^{2-} adsorption onto the precursor, a small crystalline grain and higher surface area of the precursor enhance the adsorption and, hence, increase the sulfate content of the final catalyst, even if a part of sulfate is lost during thermal activation of the catalyst. Upon calcination, there is no phase transition and the presence of SO_4^{2-} species stabilizes the surface area, thus the final SO_4^{2-}/TiO_2 catalysts retain higher surface areas and higher catalytic activities.

Table 3.1 Surface area, pore volume and crystallite size of the prepared systems

Catalyst	Surface area ($m^2 g^{-1}$)		Pore volume ($\times 10^{-6} m^3 g^{-1}$)	Crystallite size (nm)	Pore diameter (nm)
	BET	Langmuir			
T	35	46	0.09	12.71	102.8
ST	91	138	0.21	9.62	92.3
STCr(3)	100	152	0.18	5.90	72.0
STMn(3)	87	134	0.15	7.09	69.0
STFe(3)	104	160	0.17	10.40	65.4
STCo(3)	90	137	0.14	11.99	62.2
STNi(3)	83	131	0.15	12.62	72.3
STCu(3)	70	106	0.15	16.06	85.7
STZn(3)	92	139	0.14	5.92	60.1
STCr(9)	128	226	0.17	6.38	53.1
STMn(9)	98	205	0.14	19.39	57.1
STFe(9)	138	250	0.17	13.56	49.3
STCo(9)	98	206	0.11	15.07	44.9
STNi(9)	95	201	0.11	18.14	46.3
STCu(9)	80	191	0.11	16.57	55.0
STZn(9)	98	216	0.11	14.86	44.9

Addition of transition metal species causes a further setback to the crystallization and sintering process, which is evident from the higher surface area of the samples in comparison with the simple sulfated system. The metal oxide species along with the sulfate ions prevent the agglomeration of titania particles resulting in a higher surface area. Only exception is STCu(3) and STNi(3) samples for which there was a slight lowering of surface area compared to ST. Among the different metal incorporated systems, there was

no significant variation in the surface area value. As the metal content increases, surface area is found to increase. The dispersed metal oxides along with the sulfate species prevent the agglomerization of titania particles leading to an enhanced surface area.

Table 3.2 Surface area, pore volume and crystallite size of the prepared systems

Catalyst	Surface area ($m^2 g^{-1}$)		Pore volume ($\times 10^{-6} m^3 g^{-1}$)	Pore diameter (nm)
	BET	Langmuir		
STCr(6)	123	199	0.17	55.3
STMn(6)	89	180	0.12	53.9
STFe(6)	128	221	0.17	53.1
STCo(6)	91	186	0.11	48.4
STNi(6)	85	179	0.13	61.2
STCu(6)	72	170	0.12	66.7
STZn(6)	96	189	0.12	50.0

It has been shown[17,18] that in sulfated metal oxides, some of the hydroxyl bridges originally present in dried uncalcined and unsulfated titania are replaced by the sulfate ions. On calcination, the formation of oxy bonds takes place, and results in change in the Ti-O-Ti bond strength due to attachment of the sulfate bridges. Thus the changes in the Ti-O-Ti bond strength may be responsible for the formation of porous network. Consequently, the increase in surface area with an increase in sulfate content appears to be due to the stabilizing effect of the sulfate ions. In general, the pore volume of the samples is related to their crystallite size. The pore volume is increased as the anatase crystallite size in the samples becomes finer and more uniform. The pore volume of the different systems also remained in almost the same range. Comparatively low pore volume of metal loaded systems may be ascribed to

the blocking of the pores as the crystallites agglomerize by virtue of sintering. Assuming the pores are cylindrical, the average pore diameter is calculated using the formula: $d = 4V_P/S_p$, where d is the average pore diameter, V_p is the pore volume, and S_p is the surface area[5]. Decrease in the pore diameter is observed after sulfation. Metal incorporated samples also show a decrease in pore diameter. Colon *et al.*[4] reported that when ZrO_2 is incorporated into the titanium oxide, average pore diameter shifts slightly toward lower values, and the pore volume becomes significantly higher. It is known that the degree of agglomeration at constant pore diameter can be controlled by the concentration of the free hydroxide in the particle without the decrease of the number of bonds between particles[19]. Accordingly, this type of agglomeration occurring in TiO_2/SO_4^{2-} indicates that the free OH bind sites of $Ti(OH)_4$ in the particle, where the agglomeration/crystallization takes place during calcination, are consumed by the addition of SO_4^{2-} ion.

III. ENERGY DISPERSIVE X-RAY FLOURESCENCE ANALYSIS (EDX)

Elemental composition of the prepared catalytic systems is presented in table 3.3. Sulfated titania shows a sulfate content of 4.66%, while that of STCr(3) shows 9.16%. The sulfate content of the metal incorporated sample is considerably higher, when compared with sulfated titania, which indicate that metal doping brings about a considerable reduction in the extent of sulfate loss from the catalyst surface. Though the same concentration of sulfuric acid solution was used for sulfate modification of all the samples, their sulfate retaining capacity is different. The presence of these metal oxides stabilizes the sulfate over layers on the catalyst surface, which is apparent from the increase in the sulfate retaining capacity. The sulfate content for the various systems remained in the range 7.47 to 12.85%. Chromia loaded sample shows maximum sulfate retention capacity. The amount of sulfate retained in the samples shows a gradual increase as the metal content is increased. The

metal content of different systems clearly indicates that the expected catalyst profile can be successfully achieved by the present preparation method. From the results, it is evident that in all the cases, the amount of metal in the samples is very close to the expected value.

Table 3.3 Elemental composition from EDX (%)

Catalyst	TiO_2	SO_4	Metal	Catalyst	TiO_2	SO_4	Metal
T	100	-	-	ST	95.34	4.66	-
STCr(3)	88.05	9.16	2.78	STCr(6)	83.59	10.52	5.90
STMn(3)	90.49	7.28	2.23	STMn(6)	86.12	8.24	5.64
STFe(3)	89.44	7.83	2.98	STFe(6)	86.32	7.92	5.76
STCo(3)	89.81	7.83	2.36	STCo(6)	87.09	7.99	4.92
STNi(3)	89.43	8.34	2.23	STNi(6)	86.55	8.37	5.08
STCu(3)	89.89	7.47	2.67	STCu(6)	86.35	8.05	5.60
STZn(3)	89.11	8.14	2.75	STZn(6)	87.23	8.37	4.40
STCr(9)	81.60	10.58	7.82	STNi(9)	79.09	12.85	8.06
STMn(9)	83.52	9.64	6.84	STCu(9)	79.42	11.97	8.61
STFe(9)	82.92	10.21	6.81	STZn(9)	82.77	10.18	7.05
STCo(9)	80.18	11.30	8.52				

IV. SCANNING ELECTRON MICROSCOPY (SEM)

Regarding the morphology, figure 3.4 present the selected SEM images of the prepared catalysts. In SEM pictures spherical aggregates of small sub particles are observed. Particles present homogenous morphology and similar distribution in size and shape. The particle shape is spherical, but the particles are coagulated each other, and thus, the size of single particle could not be calculated accurately. The particles were clustered together due to the electrostatic effect of very fine particles. This is a very common phenomenon in

the case of nanoparticles[20]. However, it is confirmed that the particle size was distributed around 10 to 50 nm. Incorporation of transition metals does not alter the structure of titania. Particle size is observed to be larger in the case of pure titania. Crystallite size is decreased after sulfate incorporation. Addition of transition metals again changes the morphology greatly. Comparatively large particle size is observed in the case of nickel and copper loaded samples.

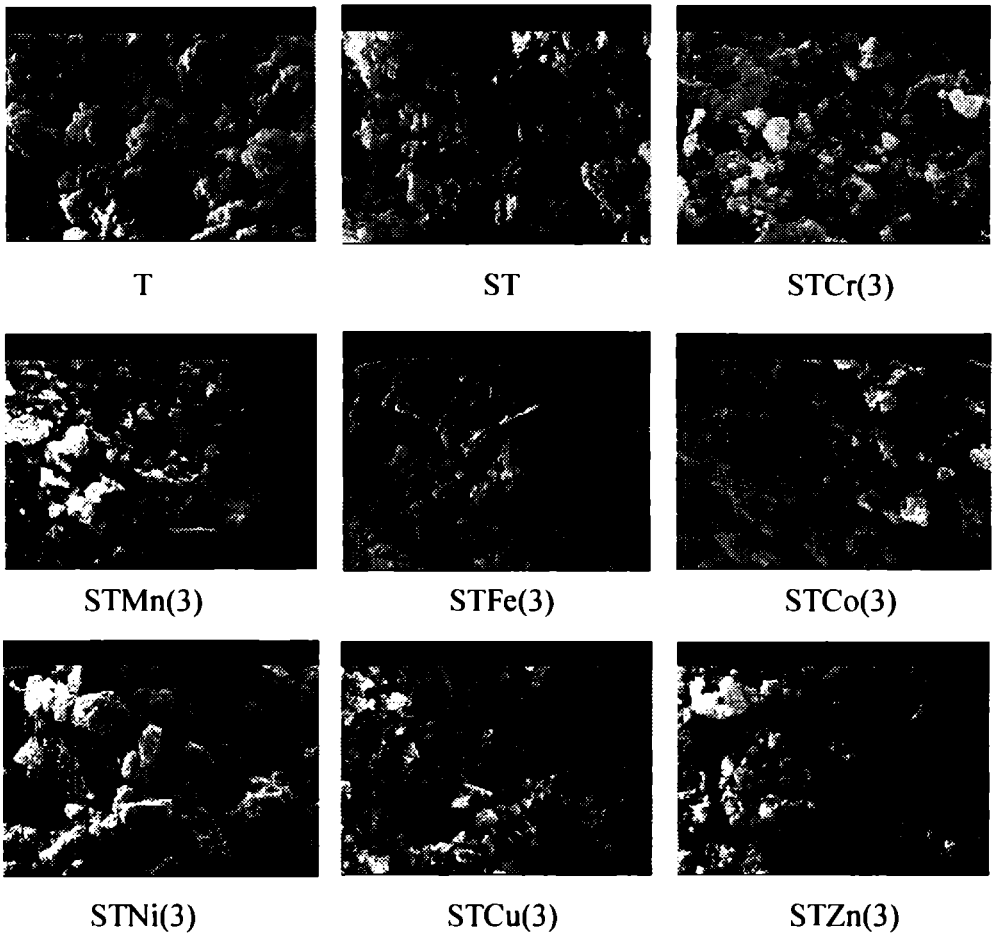

Figure 3.4 Scanning electron micrographs of representative systems

V. THERMOGRAVIMETRIC ANALYSIS (TGA)

Thermogravimetric analysis of representative samples heated under a flow of nitrogen can be seen in figures 3.5 and 3.6. The mathematically obtained differential curve is also plotted in order to clarify the weight loss processes. TG/DTG pattern of pure titania indicates a continuous dehydration over the entire temperature.

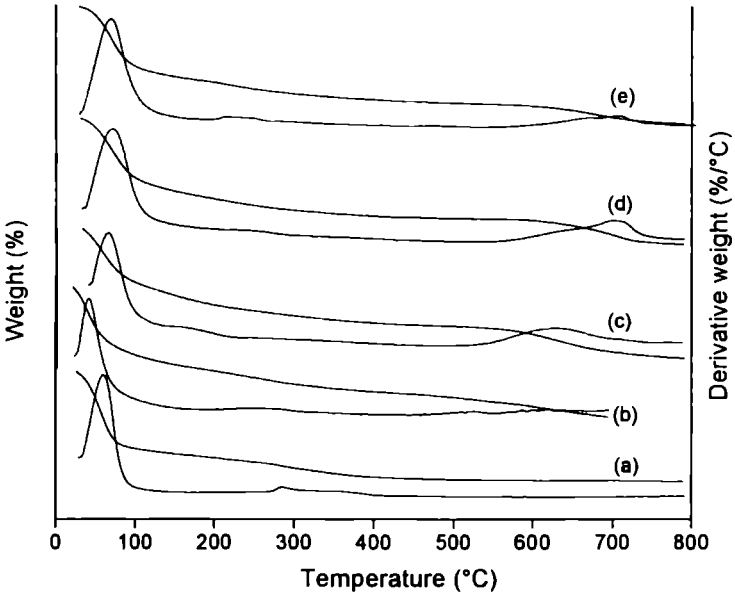

Figure 3.5 TG/DTG profiles of (a) T (b) ST (c) STCr(3) (d) STMn(3) (e) STFe(3)

The first loss of weight associated with hydration water, located between the particles, occurs in a wide temperature range, i.e., between room temperature and 100°C[21]. Another small dip in the region of 250 to 300°C may be due to the removal of structural water present in the sample. No additional weight loss is noticed in the higher temperature region in the case of pure titania. An additional decomposition in the case of sulfated samples is seen around 650-700°C and can be ascribed to the decomposition of the sulfate

species giving rise to evolution of oxides of sulfur[22]. The decomposition of surface sulfate groups above 700°C is reported in the case of sulfated metal oxide[23,24]. Here also the initial weight loss corresponds to the removal of surface adsorbed water of hydration. The metal incorporated samples exhibited a higher thermal stability. The commencement of decomposition in these cases occured only above 700°C. It is inferred that besides delaying the crystallization process, the addition of the metal species also serves to stabilize the surface sulfate species. In all these thermograms no apparent weight loss is observed up to 600°C after transformation of metal salts to corresponding metal oxide.

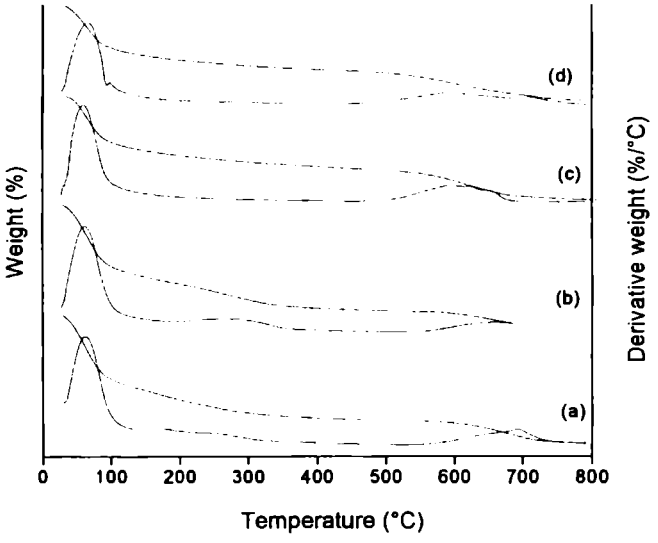

Figure 3.6 TG/DTG profiles of (a) STCo(3) (b) STNi(3) (c) STCu(3)(d) STZn(3)

VI. FOURIER TRANSFORM INFRARED (FTIR) SPECTROSCOPY

Figures 3.7 to 3.9 present the FTIR spectra of representative systems of sulfated titania catalysts calcined at 500°C. The IR spectrum of pure titania shows two strong absorption bands at 3436 and 1626 cm^{-1}. Additional bands at

around 400-500 cm^{-1} are also observed. The oxide supports generally terminate with surface OH groups, which are quite polar and give strong IR bands in the 3000-4000 cm^{-1} and 1600-1700 cm^{-1} regions[25]. The vibration modes of anatase skeletal O-Ti-O bonds are observed in the range of 400-900 cm^{-1} with a maximum at 474 cm^{-1} [26,27]. In the low energy region of the spectrum the bands at 595 and 467 cm^{-1} are assigned to bending vibrations of Ti-O bonds[28]. It was reported[29] that the bands at 1132, 979, 776and 669 cm^{-1} can be assigned as Ti-O asymmetric and symmetric stretching vibrations. The sulfate sample show IR spectra which are different from those of metal sulfates; the material show absorption bands at 980-990, 1040,1130-1150 and 1210-1230 cm^{-1}, which are assigned to the bidentate sulfate coordinated to the metal[30].

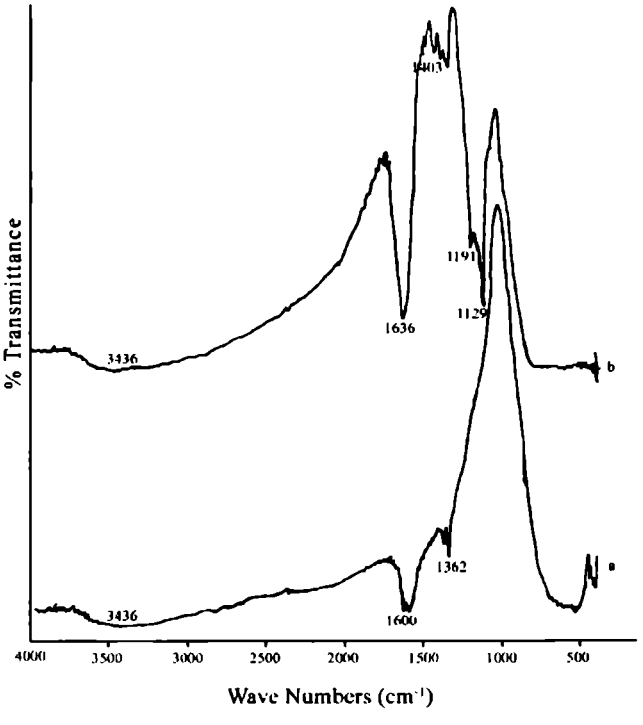

Figure 3.7 FTIR spectra of (a) T (b) ST

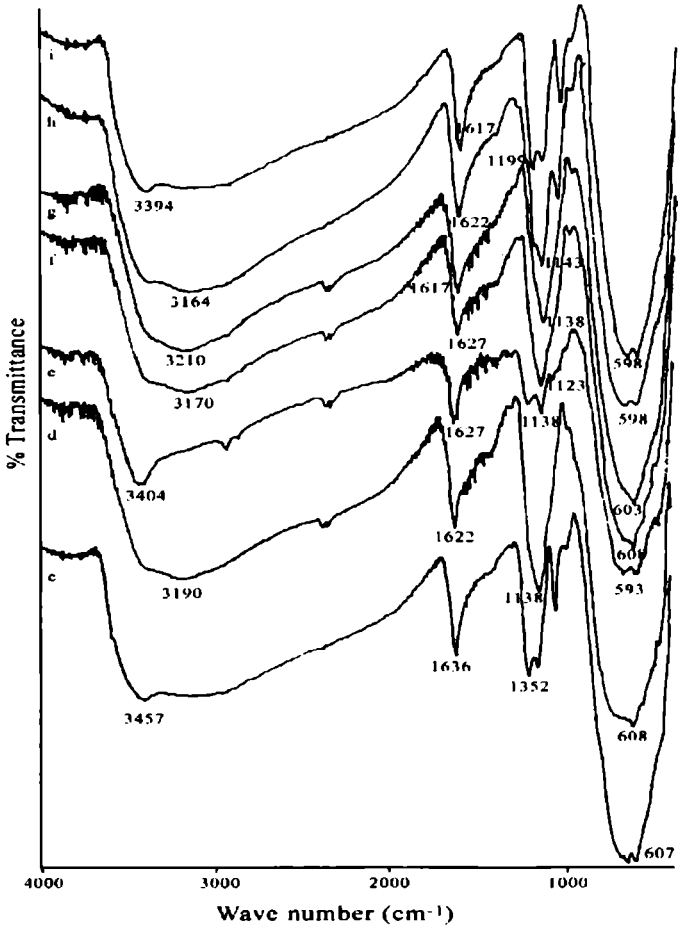

Figure 3.8 FTIR spectra of (c) STCr(3) (d) STMn(3) (e) STFe(3) (f) STCo(3) (g) STNi(3) (h) STCu(3)(i) STZn(3)

IR spectra of sulfated metal oxides gave a strong absorption band near 1380-1360 cm^{-1} and a broad band around 1000-1200 cm^{-1}. It has been reported that TiO_2/SO_4^{2-} give the bands of S=O at 1375 cm^{-1}. The drastic shift of the IR band indicates a strong interaction between the support and the surface sulfur complex[31]. The band around 1370 cm^{-1} arises from the highly covalent character of the S=O on a highly dehydrated oxide surface[24].

According to Morterra *et al.*[32] the peaks in this region correspond to isolated surface sulfates whereas generation of polynuclear sulfates at high sulfate loadings shifts the peak to around 1400 cm^{-1}. The absence of peaks around 1400 cm^{-1} suggests the absence of polynuclear species in the samples irrespective of high sulfate loading.

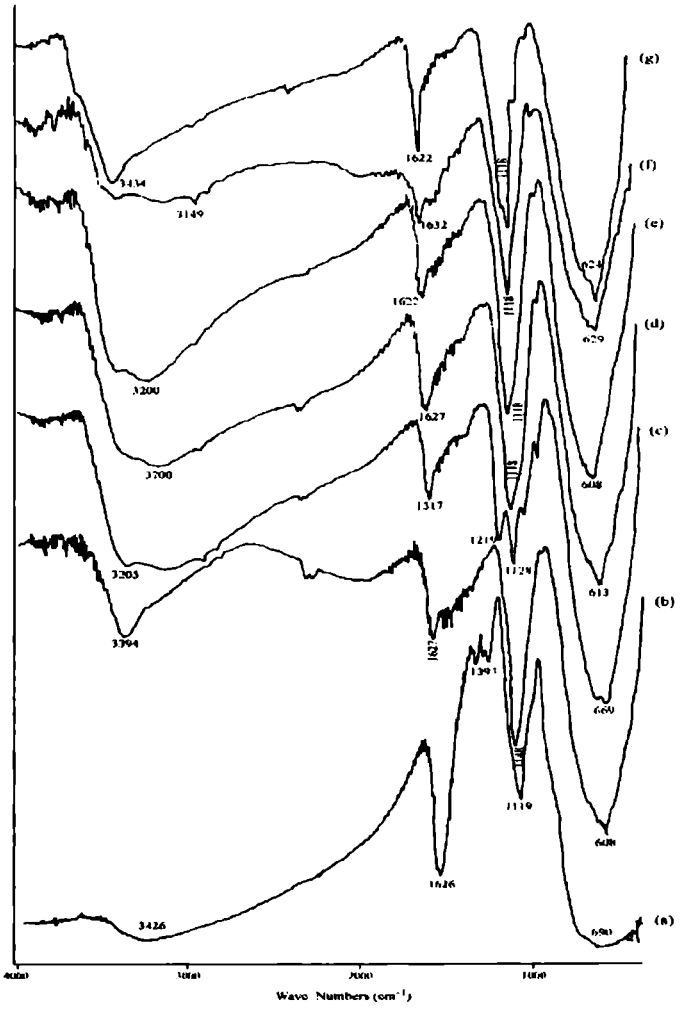

Figure 3.9 FTIR spectra of (a) STCr(9) (b) STMn(9) (c) STFe(9) (d) STCo(9) (e) STNi(9) (f) STCu(9)(g) STZn(9)

A broad band due to the –OH species appear around 3436 cm^{-1} for pure titania, whereas for the modified samples, the peak maxima is shifted. This shift in the –OH peak to a lower stretching frequency is suggestive of an enhancement in acid strength for the sulfated samples. The increase in Brönsted acidity during sulfation may be ascribed to the generation of S-OH groups[33] or to the acidity enhancement of the surface –OH groups[34]. When SO_4^{2-} is bound to the titania surface, the symmetry can be lowered to either C_{3v} or C_{2v}. The bands obtained in the 1200-1100 cm^{-1} regions are typical of sulfato complexes in a bidentate configuration with C_{2v} symmetry[35]. Thus the IR spectral bands of the samples closely agree to the bidentate sulfate complex structure having bands around 1119 and 1129 cm^{-1}.

Sulfated titania exhibits a broad IR band at the region of 3470 cm^{-1}. The absence of IR peak at 3720 cm^{-1} reveals the absence of basic hydroxyl groups. This result indicates that the surface sulfates preferentially cover the hydroxyl sites at the 3720 cm^{-1} regions, reducing the number of sites for metal loadings[14]. Saur *et al.*[24] using isotope exchange and IR analysis proposed a $(Ti\text{-}O)_3S{=}O$ structure under dry conditions for SO_4^{2-}/TiO_2. The sulfate type changes from tridentate species to bidentate species with SO_4^{2-} content on the metal oxide surface. As the sulfate loading is increased, it is proposed that $S_2O_7^{2-}$ and $S_3O_{10}^{2-}$ species may also be present[32,36-38].

VII. UV-Vis DIFFUSE REFLECTANCE SPECTROSCOPY (UV-Vis DRS)

UV-Vis spectroscopy has been utilized to characterize the bulk structure of crystalline and amorphous titania. TiO_2 is a semiconductor oxide with easily measured optical band gap. UV-Vis DRS is used to probe the band structure, or molecular energy levels, in the materials since UV-Vis light excitation creates photogenerated electrons and holes. Information about the absorptive properties of metal oxides can be obtained from diffuse reflectance UV-Vis spectroscopy. This is very important for catalysts for photocatalytic applications

since it gives information about the bad gap of semiconductors. The UV-Vis absorption band edge is a strong function of tiania cluster size for diameter less than 10 nm, which can be attributed to the well-known quantum size effect for semiconductors[39].

Table 3.4 λ_{max} and band gap energy obtained from UV-Vis DRS analysis

Catalyst	λ_{max} (nm)	Band gap energy (eV)	Catalyst	λ_{max} (nm)	Band gap energy (eV)
T	372	3.25	ST	322	3.76
STCr(3)	316	3.83	STCr(6)	314	3.85
STMn(3)	319	3.79	STMn(6)	315	3.84
STFe(3)	324	3.74	STFe(6)	323	3.75
STCo(3)	327	3.70	STCo(6)	325	3.72
STNi(3)	330	3.67	STNi(6)	327	3.70
STCu(3)	335	3.61	STCu(6)	330	3.67
STZn(3)	317	3.82	STZn(6)	316	3.83
STCr(9)	310	3.90	STNi(9)	322	3.76
STMn(9)	314	3.85	STCu(9)	327	3.70
STFe(9)	320	3.78	STZn(9)	312	3.88
STCo(9)	321	3.77			

Zhang *et al.*[40] reported the UV-Vis spectra of titania samples calcined at different temperatures. Blue shift is observed for the absorption spectra as the calcination temperature is increased. In Table 3.4, we report the calculated values of band gap energy for all samples. Band gap energy observed for TiO_2 Degussa P25 and Hombikat UV-100 reported in the literature[41] is about 3.5 eV, depending on the anatase-rutile fraction present in the oxide. The band gap energy is found to increase after sulfate modification and metal incorporation. Figure 3.10 gives the diffuse reflectance spectra of representative samples.

Characteristic band for tetrahedrally coordinated titanium appear at about 300-400 nm. The absorption is associated to the $O^{2-} \rightarrow Ti^{4+}$ charge transfer corresponding to electronic excitation from the valence band to the conduction band. A progressive shift in the band gap absorption onset to the visible region and a decrease absorbance in UV region are noticed with increasing metal content.

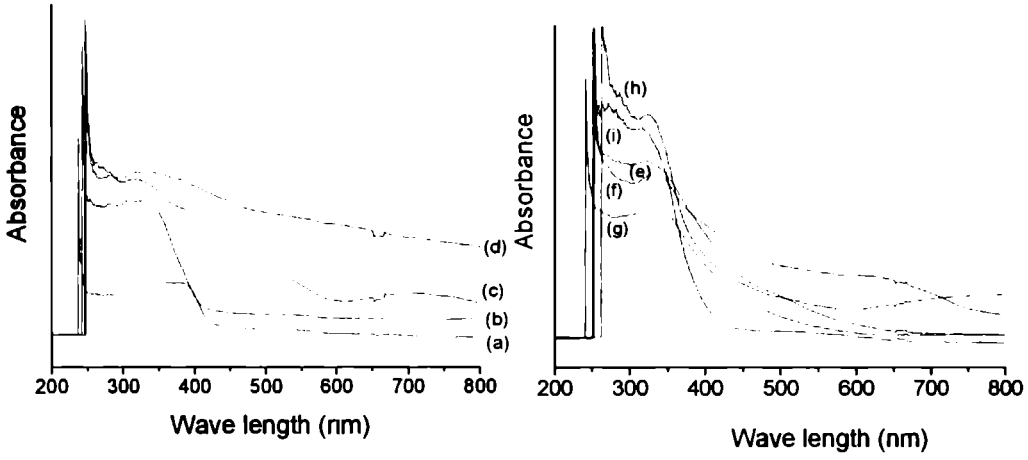

Figure 3.10 UV-Vis DR spectra of (a) T (b) ST (c) STCr(3) (d) STMn(3) (e) STFe(3) (f) STCo(3) (g) STNi(3) (h) STCu(3) (i) STZn(3)

The presence of the doping ions caused significant absorption shifts into the lower wavelength region compared to pure titania. In the case of chromium loaded samples additional band near 600 nm is observed, which is attributed to $^4A_{2g} \rightarrow {}^4T_{1g}$ transitions for Cr(III) ions in an octahedral environment[42]. However, Cr(III) →Ti(IV) charge transfer transitions, which may be alternatively described as excitation of an electron of Cr(III) into the conduction band of TiO_2, cannot be ruled out[43]. Manganese loaded samples revealed weak absorption bands in the 600-650 nm, and were assigned to the $^6A_{1g} \rightarrow {}^4T_{2g}$ crystal field transitions[44,45]. The absorption spectra of cobalt loaded samples show an increased absorption in the region of 600 nm, which may arise from charge transfer and d-d transitions[42].

VIII. SOLID STATE ^{1}H NUCLEAR MAGNETIC RESONANCE (NMR) SPECTROSCOPY

^{1}H MAS (magic angle spinning) NMR spectroscopy has proven to be an exceedingly useful technique for characterizing the hydroxylated surfaces of metal oxides. ^{1}H NMR measurements have been performed with the aim of measuring the characteristic proton chemical shifts of hydroxy groups bound to titania. Figures 3.11 and 3.12 gives the ^{1}H NMR spectra of representative samples. It is one of the best characterization techniques available for Brönsted acid amount determination as it directly probes the protons and their environments. In principle, ^{1}H MAS-NMR chemical shifts are correlated with the proton donor ability of Brönsted acid sites and hence can provide straight information about the Brönsted acidic strength[46-51].

Fraissard and coworkers[52] studied the distribution of protons between hydroxyl groups and adsorbed molecular water on different forms of tiania using a broad-line NMR technique. Recently, reports have appeared concerning the identification of hydroxy groups in mixed TiO_2-ZrO_2 supports[53]. Metal oxides have Brönsted acid sites involving oxygens at crystallographically different positions, i.e., bridging hydroxyls freely vibrating in small cages or channels[46]. Since the bridging hydroxyls interact with several other oxygens large broadening of peaks is observed. Perhaps, ^{1}H fast MAS-NMR spectroscopy at very high field is powerful technique for the atoms, their interactions may give rise to different downfield chemical shift in the ^{1}H NMR spectra, mostly reflecting an increase in Brönsted acidic strength[50,51]. Proton-proton interactions will also cause extreme line broadening and lowered resolution when the zeolite cages contain a high density of protons[47].

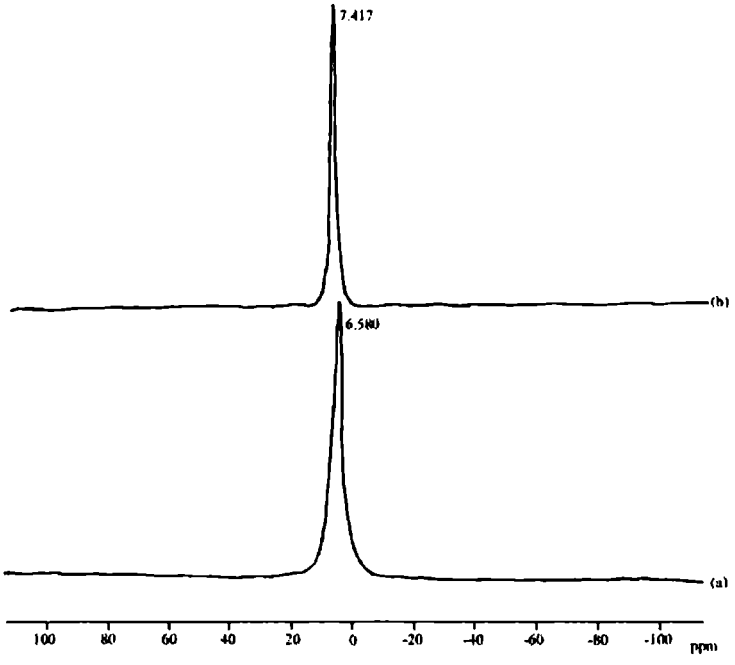

Figure 3.11 ^{1}H NMR spectra of (a) T (b) ST

Pure titania contains a major signal at δ=7.417 ppm, which is assigned to the bridging titanol group. These chemical shifts show good agreement with those of δ=6.4 ppm reported by Mastikhin, Nosov and co-workers[54-56] for anatase samples prepared by either precipitation from aqueous $TiCl_4$ or pyrolysis of $TiCl_4$. No signal corresponding to terminal titanol group is observed in any of the samples, which usually appears at δ=2.3 ppm[57]. After sulfation, the signal shift to δ=6.58 ppm, consistant with the greater acidity expected for sulfated titania and an increase of the OH bond strength. Chemical shifts of transition metal loaded samples were between -2.23 to 5.45 ppm. The relative large shift of the signal in the case of metal oxides could be taken as an indication of high Brönsted acidity[51,58]. Low chemical shift can be due to low acidity of the samples.

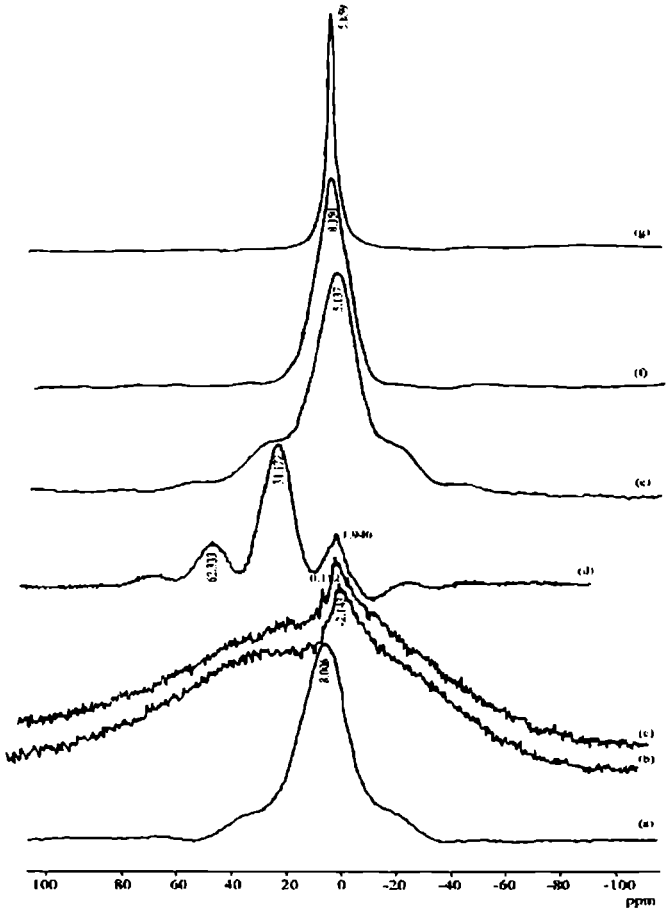

Figure 3.12 ^{1}H NMR spectra of (a) STCr(6) (b) STMn(3) (c) STFe(3) (d) STCo(3) (e) STNi(3) (f) STCu(3) (g) STZn(3)

Manganese and iron loaded samples show relatively complex spectrum. The central Brönsted acid peak becomes completely featureless and we cannot say anything on the trend of Brönsted acid amount of these samples. We can interpret this in terms of the paramagnetic influence of the metal ions used while surface modification[59]. However, we cannot overemphasize on a one-to-one correlation between chemical shift values and strength of the Brönsted acid sites. In the case of cobalt loaded sample additional signals

arise at δ=31.177 and 63.33 ppm; these signals may correspond to hydroxy groups associated with Cu-OH groups. ^{1}H NMR of rutile samples contains signals at δ=6.9 (weak) and 5.3 ppm and are assigned to bridging hydroxyl groups. The peak at lower field corresponds to hydrogen bonded hydroxy groups, i.e., they correspond to bridging hydroxy groups located on different crystallographic planes[57].

3.3 SURFACE ACIDITY MEASUREMENTS

In reactions occurring by acid catalysis, the activity, stability and selectivity of solid acids are obviously determined to a large extent by their surface acidity. The acidic properties of the metal oxides are generally thought to play an important role in determining the adsorptive and catalytic properties of these materials. Acidity is found be the most important catalytic function of sulfated oxides. Hence determination of the acid sites exposed on the surface as well as their distribution is an essential requirement to evaluate the catalytic properties of acidic solids. The effect of incorporation of various transition metals on sulfated titania and their disparity in the surface acidity were investigated in detail by employing different methods.

It is known that the acidic properties of sulfate modified metal oxides are remarkably higher than that of the pure oxide. The generation of acid sites by sulfation has been explained by the inductive effect due to the difference in the electronegativity between metal oxides and sulfate ion. In the sulfate ion the S=O structure is essential for the generation of acidic sites on sulfate promoted oxide samples. The strong ability of S=O in sulfate complexes to accommodate electron from a basic molecule is a driving force in the generation of strong acid properties. Recent studies of supported sulfate catalyst suggest that the kind of sulfate species and acidic properties depend on the nature of the oxide[24,60,61]. In order to identify the state of the sulfur species on the surface of TiO_2, the sulfated supports were examined by Choo *et al.*[14] by XPS and found

that the sulfur is existing in a form of sulfate (SO_4^{2-}) on the catalyst surface. The bidentate sulfate on the surface of TiO_2, whether chelating or bridging, has been generally proposed as the structure of sulfur[62,63].

I. TEMPERATURE PROGRAMMED DESORPTION (TPD) OF AMMONIA

Temperature programmed desorption of simple bases is a widely used method to assess the total number and strength of acid sites[64,65] Basic molecules such as ammonia[66,67,68], pyridine[64] and *n*-butylamine are the generally used probe molecules. Among these molecules ammonia is most widely used; being a small molecule, it has greater accessibility to almost all acidic sites including the weak ones. Berteau *et al.*[69] have proposed that the desorption signals below 200°C correspond to weak acidity, those between 200 and 400°C to medium strength sites, and above 400°C the signal is associated to strong acidity in the case of NH_3-TPD. Tables 3.5 and 3.6 give the distribution of acid sites of pure titania and sulfated titania systems determined by ammonia TPD method.

Pure titania possesses comparatively very small amount of acidity. Upon sulfation, it is observed that, the amount of ammonia desorbed from all the temperature region is increased considerably. Samantaray *et al.*[5] also reported the same observation over sulfated titania.It is reported in literature[70] that the maxima in the TPD profile around 535°C is attributed to desorption of NH_3 from the strong acid sites and the peak at 202°C corresponds to the weakly adsorbed NH_3. The plateau area in the temperature region 270-450°C is attributed to the desorption of NH_3 from the medium-strong acid sties in the case of sulfated titania. Acid sites are the interaction product of TiO_2 with sulfate ions. The S=O structure is essential for the generation of acidic sites on sulfate promoted oxide samples. The strong ability of S=O in sulfate complexes to accommodate electrons from a basic molecule is a driving force in the generation of highly acidic properties[71,72].

Table 3.5 Influence of the type of metal loaded on the acid site distribution of sulfated titania system

Catalyst	Amount of ammonia desorbed (mmol g^{-1})			
	Weak (100-200°C)	Medium (200-400°C)	Strong (400-600°C)	Total (100-600°C)
T	0.31	0.20	0.01	0.52
ST	0.50	0.32	0. 09	0.91
STCr(3)	0.56	0.59	0.29	1.44
STMn(3)	0.50	0.41	0.12	1.03
STFe(3)	0.48	0.32	0.15	0.95
STCo(3)	0.49	0.34	0.10	0.93
STNi(3)	0.49	0.39	0.04	0.92
STCu(3)	0.50	0.38	0.06	0.94
STZn(3)	0.50	0.34	0.15	0.99

The total acidity values obtained from ammonia TPD were comparable for the different metal incorporated systems. In fact, no correlation could be obtained between the sulfate content of the various samples and their total acidity values. STCr(6) is the one that has the maximum acidity value compared to other systems. Among the different metal loadings, 6% loaded systems show maximum acidity. This can be due to the uneven charge distribution of Ti-O-M bonds, which can donate electrons to stabilize the S=O stretching[73]. The acidic properties generated by the inductive effect of S=O bonds of the complex are strongly affected by the environment of the sulfate ion. Thus, it can be proposed that acid properties would be modified by both the type of S=O in the sulfate complex and the coverage of sulfate on the surface.

Table 3.6 Influence of the amount of metal loading on the acid site distribution of sulfated titania system

Catalyst	Amount of ammonia desorbed (mmol g^{-1})			
	Weak (100-200°C)	Medium (200-400°C)	Strong (400-600°C)	Total (100-600°C)
STCr(6)	0.75	0.67	0.31	1.73
STMn(6)	0.50	0.66	0.28	1.44
STFe(6)	0.44	0.53	0.30	1.27
STCo(6)	0.51	0.52	0.12	1.15
STNi(6)	0.50	0.55	0.08	1.13
STCu(6)	0.54	0.54	0.09	1.17
STZn(6)	0.50	0.53	0.29	1.32
STCr(9)	0.42	0.47	0.02	0.91
STMn(9)	0.37	0.46	0.01	0.84
STFe(9)	0.36	0.34	0.03	0.73
STCo(9)	0.37	0.35	0.01	0.73
STNi(9)	0.37	0.35	0.00	0.72
STCu(9)	0.38	0.35	0.00	0.73
STZn(9)	0.36	0.35	0.03	0.74

Samantaray *et al.*[8] reported a decrease in surface acidity at high sulfate concentrations. In our studies, systems that contain high metal content (having high sulfate amount) decrease the acidity of the system. The increased loading of sulfate on TiO_2, as evident from EDAX, can form the polynuclear type of sulfate complex and increase the coverage of the Ti metal ion by the sulfate ion. The polynuclear sulfate cannot extract as many electrons as isolated sulfate, to generate a strong acidity. It is reported in literature[74] that the generation of total and strong acidity is not affected by the type of sulfate

species, such as isolated and polynuclear, but by the coverage of the surface of the Ti by sulfate ions. Accordingly, it is concluded that the free Ti ion surrounding the sulfate is responsible for the generation of strong acid sites. With respect to the kind of acid site, it has been reported that both Lewis and Brönsted acid sites can be generated when a sulfate ion is introduced into TiO_2[61,62]. The nature of the acid sites is greatly altered by the nature of the ions incorporated into the lattice. The change in distribution may be a coupled effect of the crystalline and structural changes. The change in the acid strength distribution for the different systems may be related to the interaction of the added metal cations with the titania. According to Clearfield[33], strong Brönsted acidity is a result of the interaction between bisulfate groups and adjacent Lewis acid sites.

II. PERYLENE ADSORPTION STUDIES

The interaction of acid sites and basic probe molecules is studied to distinguish between Brönsted and Lewis type of acid sites and to determine their amount and strength. Qualitative information regarding Lewis acidity in the presence of Brönsted sites is based on the investigation of the ability of the surface to accept a single electron. Polyaromatic hydrocarbons such as perylene, pyrene and chrysene have mainly been used as electron donors [75,76]. The adsorption of perylene from a solution in benzene was carried out at room temperature. Perylene being an electron donor can transfer its electron to the Lewis acid sites and get itself adsorbed as perylene radical cation[77]. As the concentration of perylene in the solution increases, amount adsorbed also increases up to a certain limiting value after which it remains constant. The limiting amount of perylene indicated the surface electron accepting capacity or the Lewis acidity of the sample. The results of the perylene adsorption studies on the different systems are presented in figures 3.13 and 3.14.

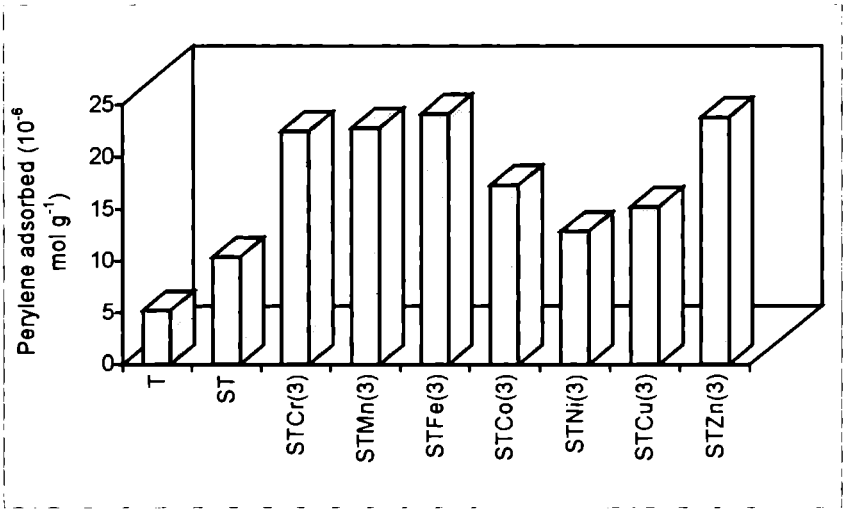

Figure 3.13 Variation of Lewis acidity from perylene adsorption studies

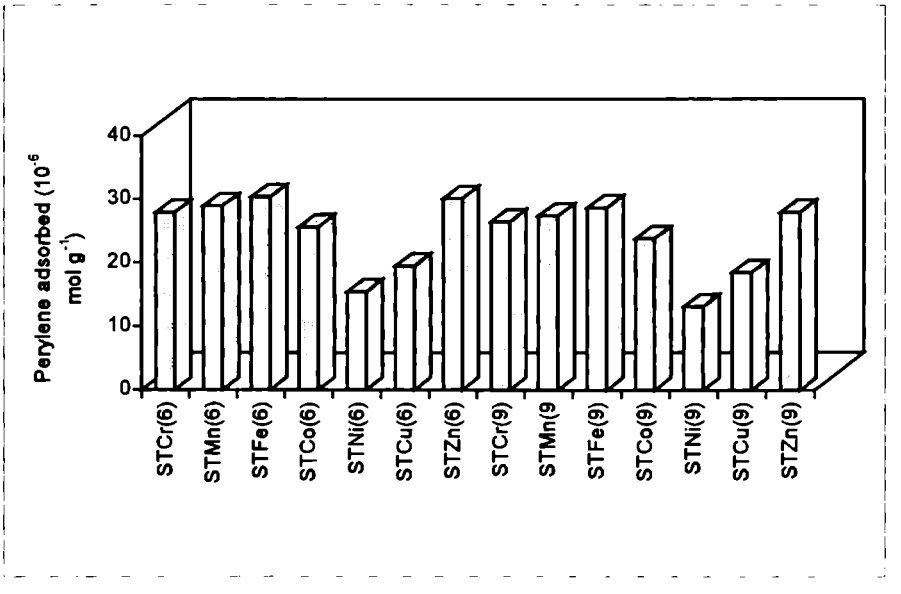

Figure 3.14 Variation of Lewis acidity from perylene adsorption studies

The results of adsorption studies clearly show a considerable enhancement of Lewis acidity on sulfation. The limiting amount of perylene

adsorbed is very low in the case of pure titania. The amount of electron donor adsorbed increases gradually when we increase the metal content from 0 to 6% and for the samples containing higher metal content, it decreases. It is generally agreed that most sulfate groups which form on the exposed patches of regular crystalline planes can induce protonic acidity, especially if they are in the form of complex polynuclear sulfates whose formation is favoured at high loadings[78]. Lewis acidity enhancement upon sulfate doping can be ascribed to the increase in the electron acceptor properties of the three co-ordinated titania cations *via.* the inductive effect of the sulfate anions, which withdraw electron density from the titanium cations through the bridging oxygen atom[79,80]. According to the duel Brönsted-Lewis site model proposed by Clearfield[33] uncalcined catalyst contains protons as bisulfate and as hydroxyl groups bridging to metal ions. During calcination, either the bisulfate anion can react with an adjacent hydroxyl group resulting in a Lewis acid site or adjacent hydroxyl groups can keep bisulfate ion intact thereby generating Brönsted acidity. The combination of these Brönsted sites with the adjacent Lewis sites can also generate strong acidity.

Incorporation of metal ions into the crystal lattice may result in the formation of some complex structures in some local area on the surface, which results in an overall increase in the electronegativity of the surface complex[81]. Iron and zinc loaded samples show higher Lewis acidity among the metal loaded systems, where as copper and nickel loaded samples show lower Lewis acidity. The variation of metal content on Lewis acidity is shown in figure 3.15. Lewis acidity increases initially, reaches a maximum at 6% loading and decreases. The reduction in the case of high meal loaded samples may be due to the high sulfate loading where sulfate groups mostly exist in the form of polynuclear species[78].

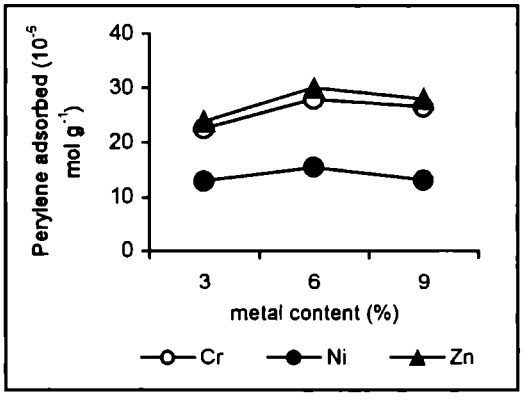

Figure 3.15 Variation of metal content on Lewis acidity

III. THERMODESORPTION STUDIES OF 2,6-DIMETHYLPYRIDINE

2,6-Dimethylpyridine (2,6-DMP) is a useful probe molecule for the selective determination of Brönsted acid sites. Corma *et al.*[82] reported that the IR bands corresponding to dimethyl pyridine associated with Lewis acid site disappeared with an increase in desorption temperature. The selective adsorption of 2,6-DMP on Brönsted acid sites is attributed to the steric hindrance of the methyl group. Satsuma *et al.*[83] reported a complete elimination of the co-ordinatively adsorbed 2,6-DMP on Lewis acid sites after purging at an appropriate temperature (above 300°C). Thus, we presume that the amount of 2,6-DMP desorbed at temperatures above 300°C originates exclusively due to desorption from Brönsted acid sites. The results of desorption studies are presented in tables 3.7 and 3.8.

The TG pattern of the samples were recorded after adsorption of 2,6-DMP to have a better understanding of the nature of surface acidity. Upon thermal treatment, 2,6-DMP gets desorbed at different temperature ranges depending on the strength of the acidic sites on which they are adsorbed. Those molecules adsorbed at strong acid sites desorbs only at high temperatures while those adsorbing on weak and medium acidic sites desorbs

at relatively low temperatures. Desorption below 300°C was omitted in the calculation since it contains contribution from Brönsted as well as weak Lewis acid sites. So as a crude approximation, it may be assumed that the desorption in the range 300 to 400°C arises from the weak sites and those in the range 400 to 500°C corresponds to medium acid strength while the strong acid sites give desorption between 500 to 600°C.

Table 3.7 Influence of the type of metal loaded on the Brönsted acid sites distribution from 2,6-DMP thermodesorption studies

Catalyst	Relative weight (%) loss of 2,6-DMP desorption			
	Weak (300-400°C)	Medium (400-500°C)	Strong (500-600°C)	Total (300-600°C)
T	0.13	0.45	0.19	0.77
ST	0.74	2.30	2.13	5.17
STCr(3)	1.03	2.61	1.96	5.60
STMn(3)	0.33	1.44	0.76	2.53
STFe(3)	0.51	1.49	0.31	2.31
STCo(3)	1.11	2.72	1.64	5.47
STNi(3)	0.84	2.51	1.78	5.13
STCu(3)	1.85	3.22	0.77	5.84
STZn(3)	0.44	1.29	1.70	3.43

From the table 3.7 it is clear that pure titania possesses only a very few Brönsted sites. Sulfated titania shows much higher Brönsted acidity compared to pure titania. Among the different metal loaded systems, copper loaded samples show the maximum Brönsted acidity. In the case of iron and zinc loaded systems the Brönsted acid sites are much less indicating that most of the acid sites are of Lewis type. Metal content also plays a beneficial role in determining the Brönsted acidity. 6% loading of the metal shows the maximum acidity and 3% loading, the minimum.

Table 3.8 Influence of the amount of metal loading on the Brönsted acid sites distribution from 2,6-DMP thermodesorption studies

Catalyst	Relative weight (%) loss of 2,6-DMP desorption			
	Weak (300-400°C)	Medium (400-500°C)	Strong (500-600°C)	Total (300-600°C)
STCr(6)	1.11	3.43	2.56	7.10
STMn(6)	0.38	0.98	2.46	3.82
STFe(6)	0.77	2.24	0.60	3.61
STCo(6)	0.97	2.38	3.23	6.58
STNi(6)	1.02	2.67	2.37	6.06
STCu(6)	1.58	2.71	3.22	7.51
STZn(6)	1.09	1.77	3.05	5.91
STCr(9)	0.75	3.25	2.04	6.04
STMn(9)	0.55	0.60	2.07	3.22
STFe(9)	0.48	1.85	0.51	2.84
STCo(9)	0.81	1.93	2.86	5.60
STNi(9)	1.00	2.33	2.15	5.48
STCu(9)	1.02	2.54	2.96	6.52
STZn(9)	0.72	1.84	2.29	4.85

IV. GAS-PHASE CUMENE CONVERSION REACTION

Cumene cracking reaction is generally used as a probe reaction to characterize the acidic properties of the catalyst. The cumene conversion and product selectivity could be correlated with the surface acidic properties. The major reaction occurring during the cumene cracking is dealkylation and dehydrogenation. Cumene is either dealkylated to benzene, dehydrogenated to α-methyl styrene, or the alkyl chain is cracked to produce ethyl benzene, toluene and styrene as shown in figure 3.15. Cracking of cumene mainly depends on Brönsted acid sties whereas dehydrogenation occurs on Lewis acid sites[84]. Thus it is possible to compare both Brönsted and Lewis acid sites in a catalyst through

cumene conversion reaction. Recently, Zenon *et al.*[85] published cumene decomposition over fluoride modified alumina. The cumene decomposition increases marginally and the selective products are benzene and propylene, while sodium modified alumina leads the cumene cracking into α-methyl styrene, which reveals that alumina surface is completely inactive in dealkylation.

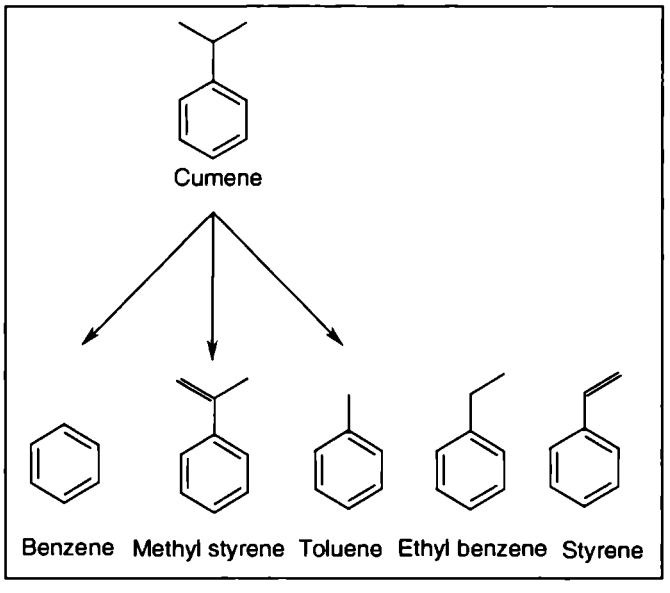

Figure 3.15 General scheme of cumene conversion reaction

1. PROCESS OPTIMIZATION

A systematic study of cumene cracking reaction was carried out in a fixed bed down flow reactor of 1.2 cm ID and 25 cm length in the optimum temperature under atmospheric pressure. 0.5 g of the catalyst activated at 500°C for 2 h was secured between two plugs of glass wool inside the reactor. The temperature was controlled by a Cr-Al thermocouple placed inside the reactor. The reactant was supplied using a syringe pump and the liquid products were collected using a condenser at required time intervals. The products were analyzed by Gas Chromatography (*Chemito 8610* using SE-30

column having FID). The total conversion is defined as the sum of all aromatics except cumene divided by the sum of all aromatics including cumene. Among the products of cumene transformation, benzene and α-methyl styrene were detected as the major products. Small amounts of toluene, ethyl benzene and styrene are also detected as side products.

I. Effect of temperature

The reaction was done in a temperature range from 300 to 450°C at a flow rate of 3 mL h^{-1}. Figure 3.16 shows the influence of reaction temperature on the conversion and selectivity pattern. As the temperature increases cumene conversion also increases. The conversion is very low initially and it becomes 14.45% at 450°C.

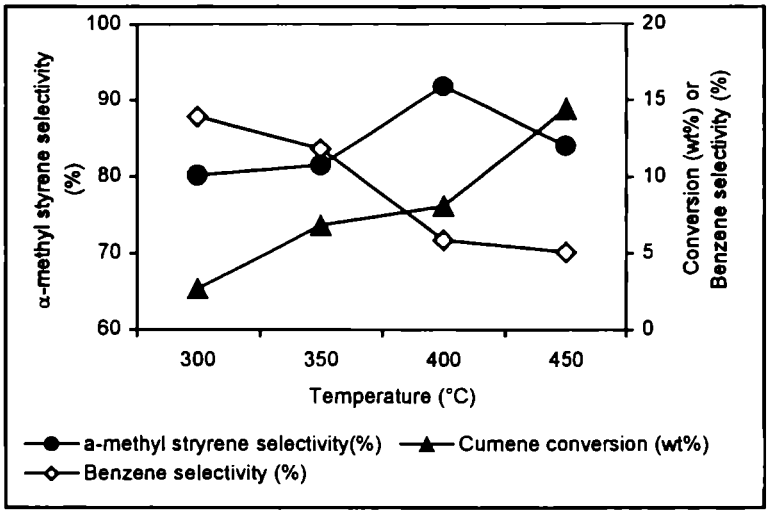

Figure 3.16 Influence of reaction temperature on cumene conversion.

Amount of catalyst: 0.5 g STMn(6), Flow rate: 3 mL h^{-1}. Reaction time: 2 h.

From the figure, it is clear that α-methyl styrene is produced to a much higher extent when compared to the formation of benzene. At 400°C, the selectivity towards α-methyl styrene increases upto 91.87% and that of

benzene decreases to 5.88%. The catalyst is possessing large number of Lewis acid sites and hence dehydrogenation was favored more. The selectivity to α-methyl styrene increases and reaches a maximum at 400°C and then decreases. As the temperature increased from 350 to 400°C some of the Brönsted acid sites are converted into Lewis acid sites resulting in the increased selectivity of α-methyl styrene at 400°C.There is an optimum temperature at which the selectivity towards α-methyl styrene is maximum. At higher temperatures the amounts of both benzene and α-methyl styrene are low, while the amount of side products are higher.

II. Effect of Flow Rate

A typical activity profile of cumene conversion as a function of flow rate over STMn(6) is shown in figure 3.17. The conversion decreases as we increase the flow rate. At higher flow rates, the contact time between the reactant and the catalyst is less, which results in less conversion. As the feed rate is increased from 3 to 6 mL h^{-1}, the conversion decreased from 8.11 to 5.82 %. The contact time between the reactant and the catalyst surface is a decisive factor in determining the activity of the catalyst. At higher flow rates the contact time will be less leading to decrease in conversion. At all flow rates major product was α-methyl styrene with small amounts of benzene, toluene, ethyl benzene and styrene. The catalyst showed above 80% selectivity to α-methyl styrene at all flow rates and this indicates that surface acidity of the system is mainly due to the Lewis acid sites. With increase in flow rate, decrease in the dehydrogenation activity is observed. Maximum selectivity for α-methyl styrene is observed at a flow rate of 3 mL h^{-1}.

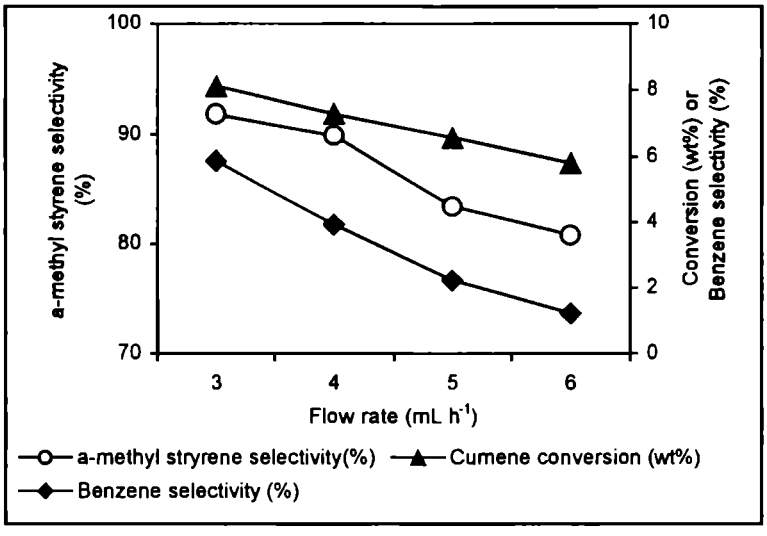

Figure 3.17 Influence of flow rate on cumene conversion and product selectivity

Amount of catalyst: 0.5 g STMn(6), Reaction temperature: 400°C, Reaction time: 2 h.

III. Effect of Time on Stream-Deactivation Study

Performance of the reaction for a continuous 7 hours run was studied to test the deactivation of the catalyst. The products were collected and analyzed after every one hour. Figure 3.18 shows that even after 7 h of reaction time, the selectivities do not vary much. In the case of metal incorporated systems, there is an increase in the selectivity initially, after that it remains almost constant. This may be due to the fact that the coke formed during the reaction may not be bulky to block all the pores of the catalyst[86].

2. COMPARISON OF DIFFERENT SYSTEMS

The cumene conversion reactions for the different catalytic systems were performed under the optimized condition. Reaction temperature-400°C, flow rate-3 mL h^{-1} and time on stream-2 h. The conversion and selectivity for various products are given in tables 3.9 and 3.10.

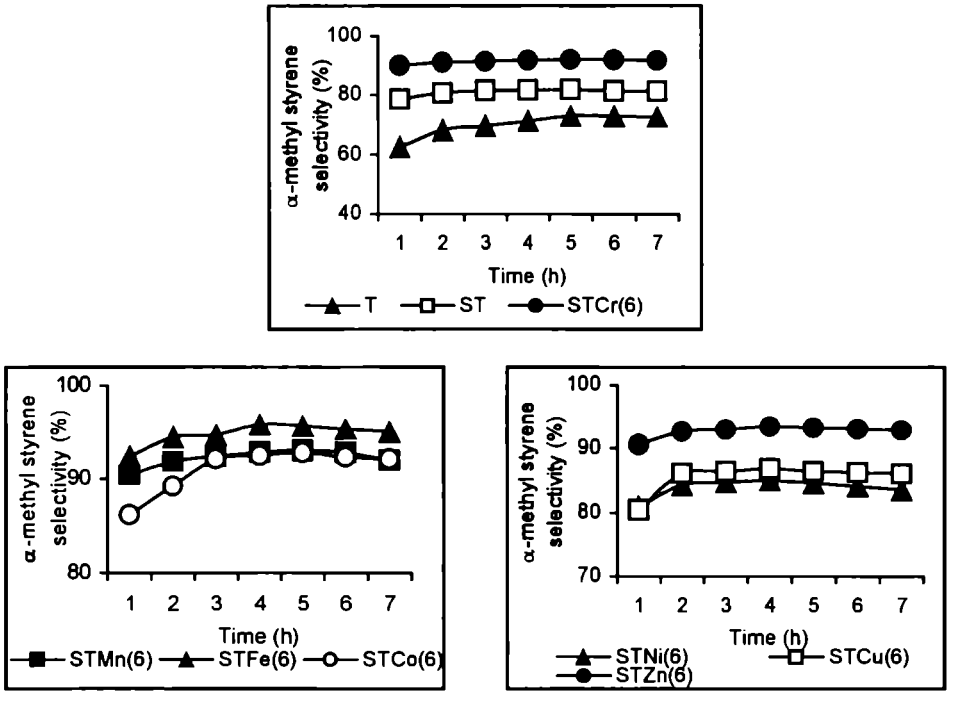

Figure 3.18 Deactivation studies on cumene conversion over different systems

Amount of catalyst: 0.5 g, Reaction temperature: 400°C, Flow rate: 3 mL h^{-1}.

In all the systems, α-methyl styrene is the predominant product, which confirms that dehydrogenation of cumene is the main reaction occurring under the reaction conditions. Compared to pure titania, metal incorporated systems are showing increased activity and selectivity. Titania possesses as very few Lewis acid sites and hence exhibits low α-methyl styrene selectivity. Maximum conversion is shown by STCr(3) while the α-methyl styrene selectivity is high for STFe(3). From tables 3.9 and 3.10 it is clear that all the systems except T are showing more than 80% selectivity for α-methyl styrene. Incorporation of transition metals, increases the Lewis acidity as revealed from perylene adsorption studies, and hence the α-methyl styrene selectivity. As the metal loading is increased, the conversion and selectivity increases up to 6% and then decreases in the case of 9% loading.

Table 3.9 Influence of the type of metal loaded in the cumene conversion

Systems	Conversion of cumene (wt%)	Selectivity (%)	
		α-methyl styrene	Benzene
T	1.31	67.93	3.60
ST	2.49	80.85	6.25
STCr(3)	5.22	86.34	7.23
STMn(3)	5.08	87.91	4.57
STFe(3)	4.80	92.44	4.20
STCo(3)	4.20	84.23	6.78
STNi(3)	2.54	81.33	5.38
STCu(3)	4.31	82.54	7.89
STZn(3)	4.36	89.48	4.93

Amount of catalyst: 0.5 g, Flow rate: 3 mL h^{-1}, Reaction time: 2 h, Reaction temperature: 400°C.

Rana *et al.*[87] studied the cumene cracking reaction over sulfided Co(Ni)Mo/TiO_2-SiO_2 catalyst and found that 8 wt% loading is optimum for maximum activity. Supporting evidence for these conclusions is provided by the ammonia TPD and adsorption studies. Cumene cracking was carried out over γ-alumina impregnated with fluoride, cobalt, molybdena and combination of these additives by Boorman *et al.*[88,89], and catalytic activities of these systems were correlated with the acidity. In the present case also we can correlate the cumene conversion with total acidity obtained from ammonia TPD measurements (figures 3.19 and 3.20).

Table 3.10 Influence of amount of metal loading in the cumene conversion

Systems	Conversion of cumene (wt%)	Selectivity (%)	
		α-methyl styrene	Benzene
STCr(6)	8.57	91.00	9.88
STMn(6)	8.11	91.87	5.88
STFe(6)	7.92	94.41	5.14
STCo(6)	6.47	89.22	8.85
STNi(6)	5.90	84.26	7.47
STCu(6)	6.92	86.12	12.11
STZn(6)	7.63	92.64	6.93
STCr(9)	2.46	87.84	7.36
STMn(9)	2.38	88.16	4.96
STFe(9)	2.35	93.53	4.50
STCo(9)	2.30	84.14	7.05
STNi(9)	2.28	82.13	6.78
STCu(9)	2.30	83.21	8.09
STZn(9)	2.35	89.08	5.27

Amount of catalyst: 0.5 g, Flow rate: 3 mL h^{-1}, Reaction time: 2 h, Reaction temperature: 400°C.

Brönsted acidity obtained from the thermodesorption of 2,6-DMP and benzene selectivity from cumene conversion shows very good correlation (figures 3.21 and 3.22). Brönsted acidity changes with respect to the metal ions and the maximum is possessed by STCu(3), and minimum by STFe(3) for 3 % loading. Benzene selectivity also follows the same trend.

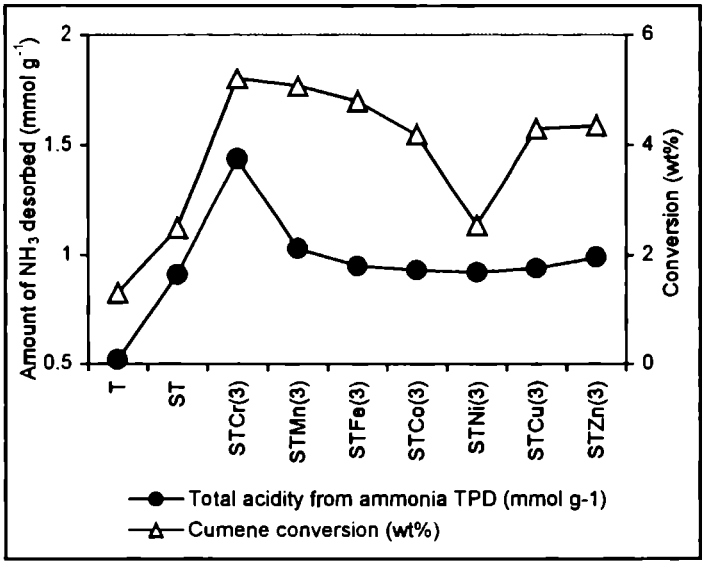

Figure 3.19 Correlation between cumene conversion and total acidity

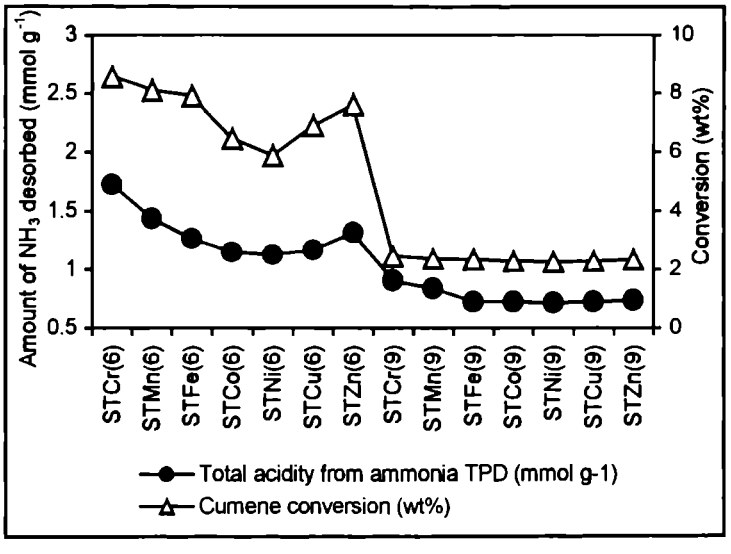

Figure 3.20 Correlation between cumene conversion and total acidity

Chromia is reported to be a strong Lewis acid[90]. The presence of chromium in the samples may lead to high Lewis acidity and hence the dehydrogenation selectivity. The comparatively high value of limiting amount for perylene adsorption also supports the high Lewis acidity of chromia containing systems. Change in the metal content also changes the selectivity. High loading of metals resulted in the decrease of percentage conversion. This can be attributed to the decrease in the acidity for the high loaded samples due to the formation of polysulfate species[17]. The inhibition of Lewis acidity due to the high loading led to the reduction of percentage selectivity of α-methyl styrene. In all the cases the selectivity to α-methyl styrene is more than 80%. All the systems show very low selectivity for benzene showing less number of Brönsted acid sites in the samples.

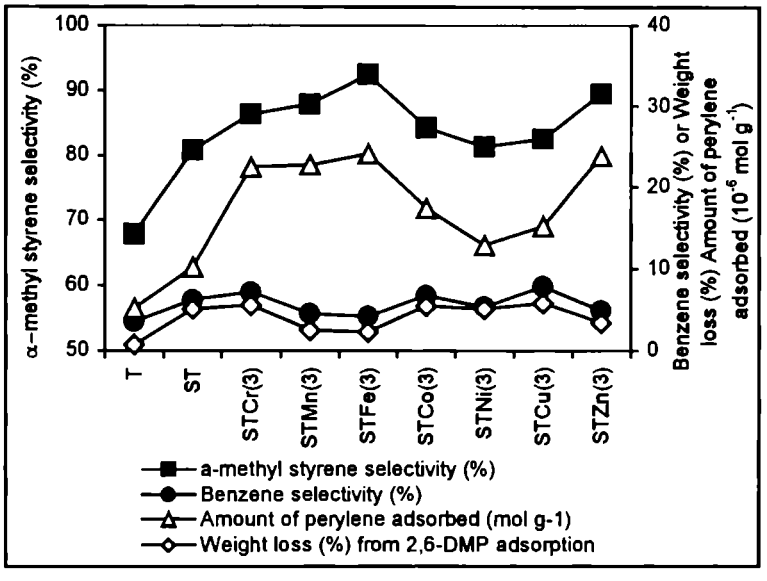

Figure 3.21 Correlation of α-methyl styrene selectivity with Lewis acidity and benzene selectivity with Brönsted acidity

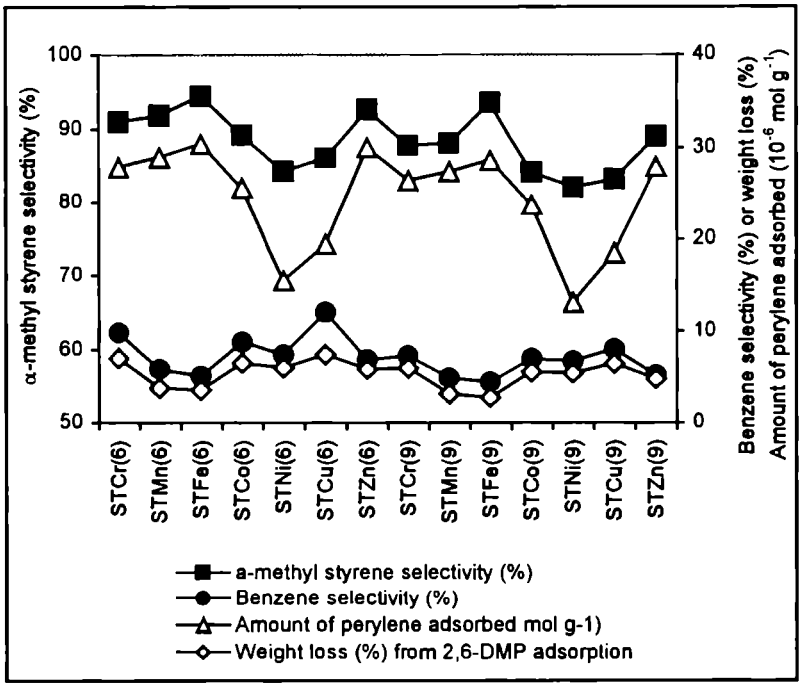

Figure 3.22 Correlation of α-methyl styrene selectivity with Lewis acidity and benzene selectivity with Brönsted acidity

3. MECHANISAM OF CUMENE CONVERSION REACTION

The major reactions occurring during cumene conversion may be grouped into dealkylation (cracking) and dehydrogenation. Cracking of cumene to benzene is generally attributed to the action of Brönsted sites by a carbonium ion mechanism[17,90-94], while dehydrogenation of cumene yields α-methyl styrene as the major product, the formation of which has been ascribed to the Lewis acid sites[17]. Corma *et al.*[95] reported that dealkylation of cumene requires the presence of a small number of Brönsted acid sites which are capable of formation of a σ-complex with cumene molecule. Bautista *et al.*[96,97] assumed the mechanism for cumene decomposition on the basis of Brönsted acid sites which is taking place by the protonation of cumene

molecule to form π-complex and subsequently this complex is transformed into σ-complex. A plausible mechanism of cumene conversion reaction is represented in figure 3.23.

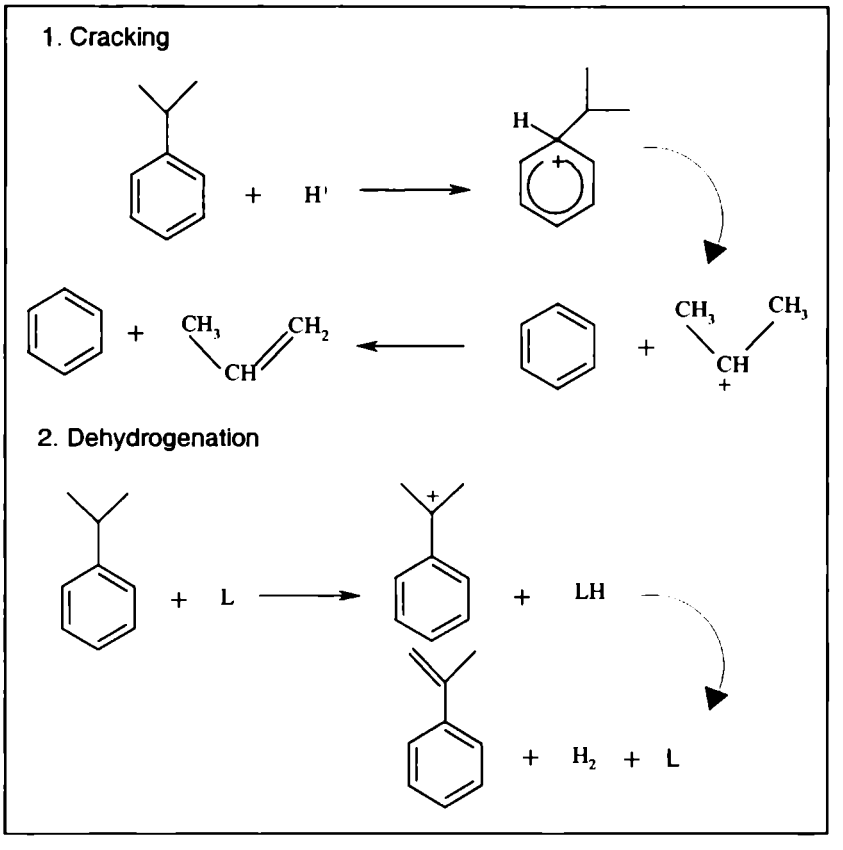

Figure 3.23 Mechanism of cumene conversion reaction

V. CYCLOHEXANOL DECOMPOSITION REACTION

Alcohol decomposition reaction is widely studied to check the acid-base property of the catalyst system[98]. The amphoteric character of the alcohol permits its interaction with both acidic and basic centers. Decomposition of isopropanol[99,100] and of cyclohexanol[101,102] are the most widely studied reactions in this category. Dehydrogenation and dehydration can take place

resulting in the formation of cyclohexanone and cyclohexene[103] (figure 3.24) in the case of cyclohexanol decomposition reaction. Dehydration activity is linked to acidic property and dehydrogenation activity to the combined effect of both acidic and basic properties.

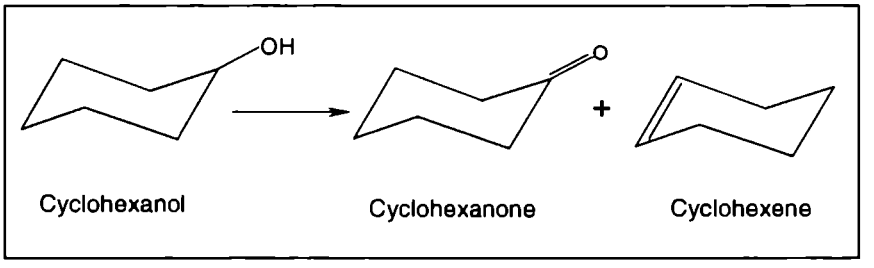

Figure 3.24 Scheme of cyclohexanol decomposition reaction

1. PROCESS OPTIMIZATION

Cyclohexanol decomposition was carried out in a continuous flow fixed bed reactor. 0.5 g of the preactivated catalyst was placed in the middle of the reactor and cyclohexanol was fed by a syringe pump at different flow rates. The temperature is monitored using a Cr/Al thermocouple placed in the middle of the reactor. The liquid products were analyzed by a *Chemito 8610* Gas Chromatograph analyzer fitted with FID using Carbowax column (2 m). The products were identified as cyclohexene, cyclohexanone, benzene, methyl cyclopentene and cyclohexane. Among these cyclohexene and cyclohexanone were the major products and the selectivities were calculated accordingly. For any catalyst system, the activity and selectivity towards a particular reaction depend on reaction parameters in addition to the physical and chemical properties of the catalysts. The optimum parameters for cyclohexanol decomposition were determined by carrying out the reaction at different temperatures and flow rates.

I. Effect of temperature

The reaction is carried out at various reaction temperatures in the range of 200-350°C. Table 3.11 shows the influence of reaction temperature on the conversion and the product distribution. As the temperature increases the percentage conversion also increases.

Table 3.11 Effect of reaction temperature on the conversion of cyclohexanol

Temperature (°C)	Conversion of Cyclohexanol (wt%)	Selectivity (%)	
		Cyclohexene	Cyclohexanone
200	72.95	90.85	8.89
250	89.46	92.24	7.02
300	97.40	93.53	6.34
350	98.58	92.83	6.54

Amount of catalyst: 0.5 g STCr(6), Flow rate: 4 mL h^{-1}, Reaction time: 2 h.

The conversion reached a maximum of 98.5% at a temperature of 350°C. Cyclohexene is found to be the major product with selectivity more than 90% at all temperatures. Increase in the temperature will decompose surface hydroxyl ions and subsequently will create more Lewis acid centers. Cyclohexanone selectivity is less, which was formed by the participation of both acidic and basic sites[104,105]. Even though there is enough number of acidic sites, absence of basic sites on the titania surface restricts the formation of cyclohexene. Cyclohexene selectivity is maximum at 300°C, and then decreases.

II. Effect of Flow Rate

A series of experiments were conducted at a reaction temperature of 300°C at different flow rates viz. 3, 4, 5 and 6 mL h^{-1} to understand the

influence of flow rate on the reaction. Figure 3.25 shows the effect of flow rate on cyclohexanol conversion and selectivity.

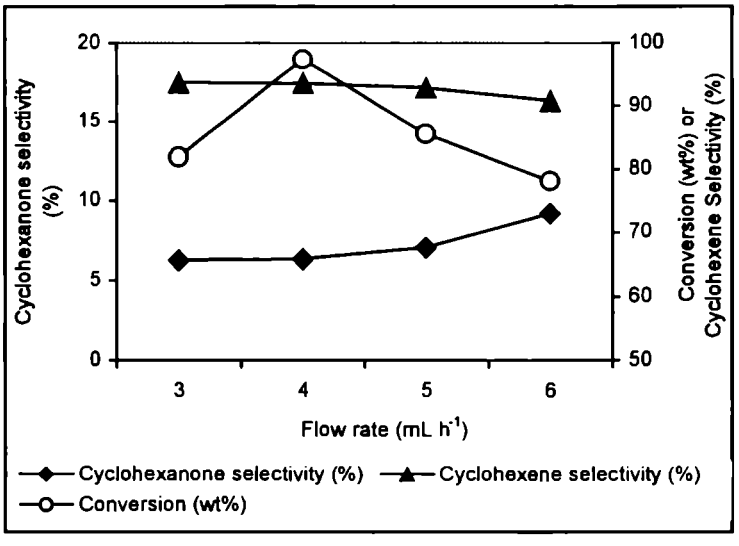

Figure 3.25 Influence of flow rate on cyclohexanol conversion and selectivity

Amount of catalyst: 0.5 g STCr(3), Reaction temperature: 300°C, Reaction time: 2 h.

Conversion increases initially as the flow rate changes from 3 to 4 mL h^{-1}, however further increase in flow rate decreases the conversion. The conversion decreases from 97.40 to 78.14%, as the flow rate increases from 4 to 6 mL h^{-1}. Decrease in contact time leads to reduction in conversion. Increase in flow rate did not alter the selectivity of catalyst to a considerable extent. At all flow rates about 90% selectivity for cyclohexene is observed. Maximum conversion and maximum selectivity is shown at 4 mL h^{-1} and is selected for further studies.

III. Effect of Time on Stream-Deactivation Study

Stability studies of different catalysts were performed by observing the conversion over a period of 7 hours. Reactions were carried at 400°C at a flow rate of 4 mL h^{-1} and the product analysis was done at regular intervals of 1 hour and is given in figures 3.26 . All systems are showing excellent activity

over a period of 3 hours after that it decreases slowly. The decrease in the activity indicates that there is some decrease in the acidity of catalyst with time. Rate of deactivation is more or less same in all the cases. Even after 7 h reaction time metal incorporated systems show more than 60% conversion.

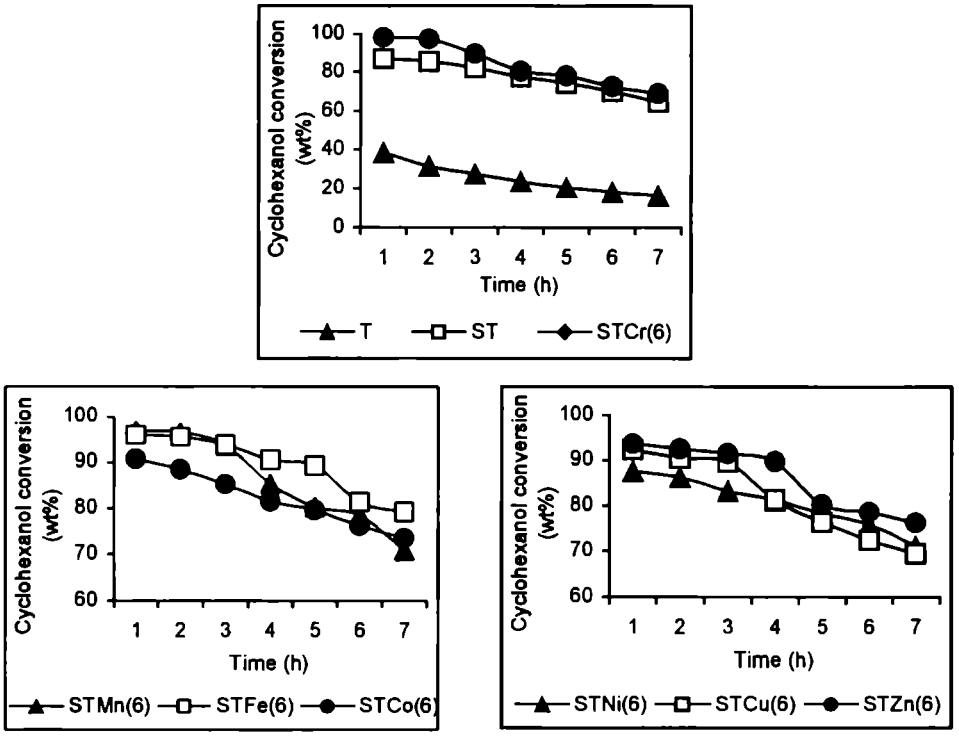

Figure 3.26 Deactivation studies on cyclohexanol decomposition over different systems

Amount of catalyst: 0.5 g, Reaction temperature: 300°C, Flow rate: 4 mL h^{-1}.

2. COMPARISON OF DIFFERENT SYSTEMS

In order to compare catalytic performance of different systems for the cyclohexanol decomposition reaction, we carried out the reaction under optimized conditions (reaction temperature-300°C, flow rate-4 mL h^{-1} and reaction time-2 h) over all the prepared systems. The results obtained are

presented in tables 3.12 and 3.13. From the tables it is obvious that the activity of the systems is greatly influenced by the presence of metal incorporated as well as the sulfate ions on the surface. Chromia loaded systems show the maximum activity. This may be due to the high acidity of these samples as evident from results of ammonia TPD.

Table 3.12 Influence of the type of metal loaded in the cyclohexanol decomposition reaction

Systems	Conversion of Cyclohexanol (wt%)	Selectivity (%)	
		Cyclohexene	Cyclohexanone
T	31.54	62.45	16.24
ST	85.36	82.36	10.10
STCr(3)	92.20	89.81	7.96
STMn(3)	91.48	87.95	8.40
STFe(3)	84.25	80.40	9.02
STCo(3)	85.54	84.32	9.28
STNi(3)	86.92	84.34	7.68
STCu(3)	87.00	86.08	9.87
STZn(3)	86.32	84.88	7.27

Amount of catalyst: 0.5 g, Flow rate: 4 mL h^{-1}, Reaction time: 2 h, Reaction temperature: 300°C.

Since pure titania possess very low acidity, its activity is also less. Depending upon the percentage of metal, selectivity also changes. The metal content also plays an important role in cyclohexanol decomposition reaction. All the sulfated systems show more than 70% conversion and high selectivity towards cyclohexene. Sulfating agents, being acidic species, preferentially attack the basic sites converting these to acidic sites[108]. The high activity in the formation of cyclohexene may be due to the weak and medium acid centers on the catalyst surface, which is apparent from ammonia TPD measurements[106].

The considerably small amount of other products like benzene, methyl cyclohpentene and cylohexane points to the absence of strong acid sites on the catalyst surface.

Table 3.13 Influence of the amount of metal loading in the cyclohexanol decomposition reaction

Systems	Conversion of Cyclohexanol (wt%)	Selectivity (%)	
		Cyclohexene	Cyclohexanone
STCr(6)	97.40	93.53	6.34
STMn(6)	96.53	90.26	7.78
STFe(6)	85.49	88.00	7.59
STCo(6)	88.48	80.34	9.74
STNi(6)	90.24	81.83	7.68
STCu(6)	95.49	88.46	6.45
STZn(6)	89.24	89.25	9.22
STCr(9)	83.56	85.39	11.61
STMn(9)	80.32	83.14	9.71
STFe(9)	72.54	70.49	9.76
STCo(9)	76.21	72.54	7.68
STNi(9)	76.75	78.26	9.69
STCu(9)	78.00	80.75	10.68
STZn(9)	73.62	74.07	6.76

Amount of catalyst: 0.5 g, Flow rate: 4 mL h^{-1}, Reaction time: 2 h, Reaction temperature: 300°C.

Gervasini and Auroax[99,107] attempted to correlate the dehydration and dehydrogenation activity of isopropanol decomposition with the acid base character obtained by the calorimetric investigation of a large series of metal oxides. Ramankutty *et al.*[105] had studied the cyclohexanol decomposition

reaction over the ferrospinels and reported that the sulfation had increased the dehydration activities of all the ferrites. Bezouhanova *et al.*[108] recommend dehydration activity of cyclohexanol decomposition as a simple method of determining Brönsted acid sites on a catalyst surface. The same opinion was also expressed by Martin and Duprez[102] and Armendia *et al.*[100]

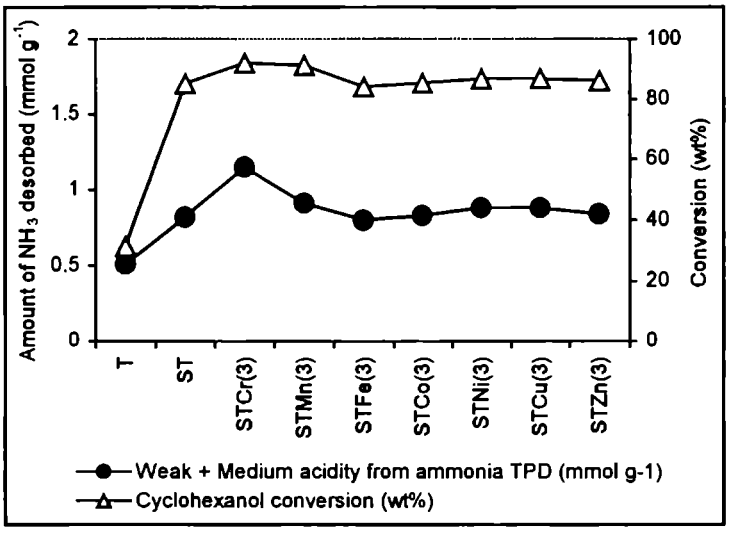

Figure 3.27 Correlation between cyclohexanol conversion and 'weak + medium' acidity from NH_3-TPD

The formation of cyclohexanone over any catalyst indicates the presence of strong and medium basic centers. The formation of cyclohexanone is low at the optimized reaction temperature indicating the absence of strong basic centers though medium and weak basic centers exist in the catalyst. But for high loadings, selectivity to cyclohexanone is found to be slightly higher. With high loadings, the basic centers might have increased which accounts for the higher selectivity to cyclohexanol. It is also confirmed by the decrease in acidity values from ammonia TPD. The selectivity in alcohol decomposition is mainly controlled by the acid-base properties[109]. Variation in the dehydrogenation and dehydration selectivity for the

catalyst systems suggests that acidic and basic properties of sulfated titania vary with incorporation of different transition metal oxides.

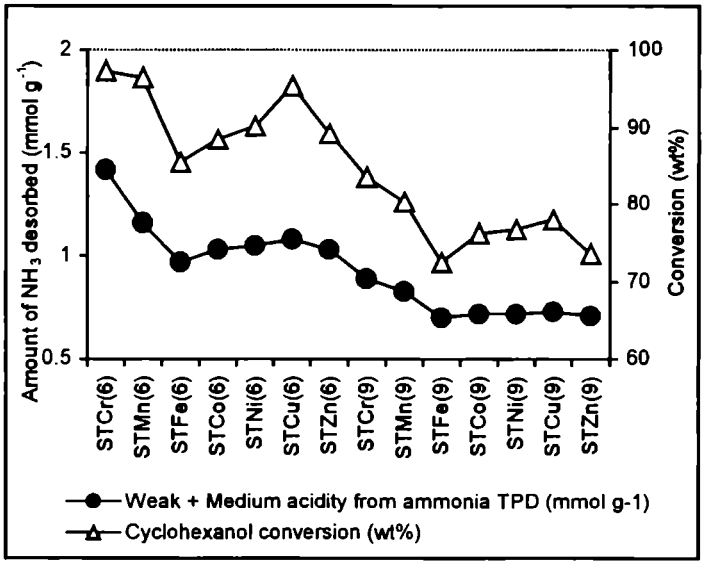

Figure 3.28 Correlation between cyclohexanol conversion and 'weak + medium' acidity from NH_3-TPD

Comparing the reaction data with various acidity data, we could find a direct relationship between the percentage conversion and the sum of weak and medium acidity obtained from ammonia TPD. Figures 3.27 and 3.28 show the correlation between the acidity and the conversion of cyclohexanol. As the percentage loading of metal increases the conversion and cyclohexene selectivity increase, but for higher loadings both decrease. On modification with sulfate ions some of the basic sites are converted to acidic sites. The mechanism of sulfation is an anion exchange between SO_4^{2-} and OH^-, which is already reported[110]. During their study of cyclohexanol conversion at 300°C, Martin and Duprez[102] noted that the presence of sulfate on zirconia increased its protonic acidity as proved by an increase in the cyclohexene selectivity. So in the case of sulfated titania systems there are enough acidic sites to catalyze the dehydrogenation giving better cyclohexene selectivity.

3. MECHANISAM OF CYCLOHEXANOL DECOMPOSITION REACTION

Cyclohexanol dehydration leads to cyclohexene whereas dehydrogenation gives cyclohexanone. It has been well established that Brönsted acid sties of the catalyst are directly involved in the alcohol dehydration mechanism. It is similar to E-1 elimination in which the reaction proceeds through initial formation of carbocation.

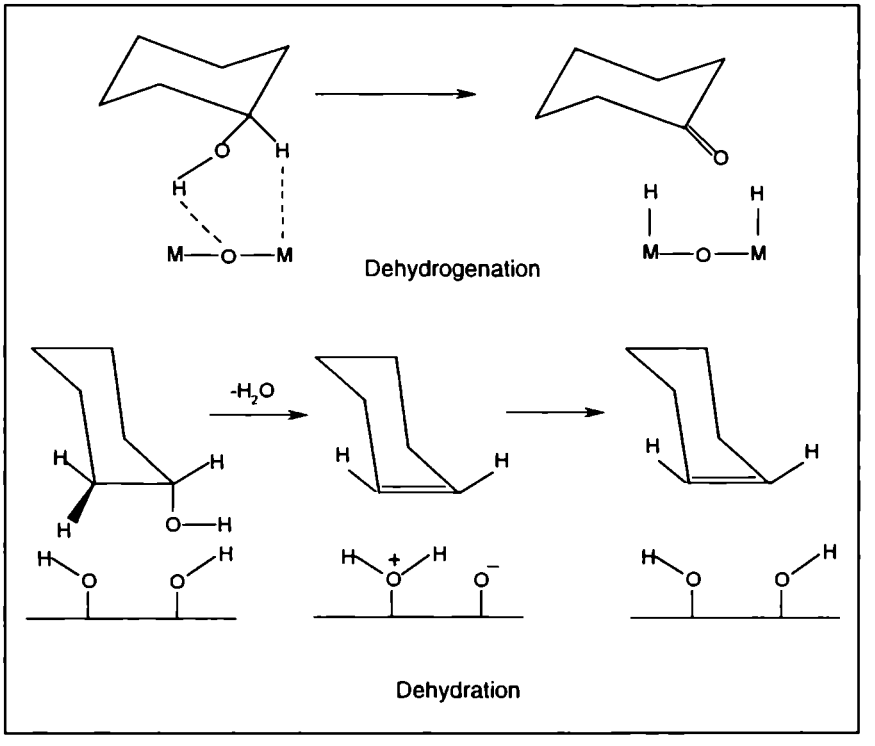

Figure 3.29 Mechanism of dehydrogenation and dehydration of cyclohexanol on oxide surface

In the case of dehydrogenation, the fission of the O-H and C_α-H bond is involved. The metal cation is acting as a Lewis acid site accepting a hydride ion whereas the oxygen anion of the catalyst is acting as a Brönsted base accepting the proton of the OH group of the alcohol[111,112]. The mechanism of dehydration and dehydrogenation of cyclohexanol is given in figure 3.29. In

addition to cyclohexene and cyclohexanone, trace amount of phenol, benzene and cyclohexane were also detected. Benzene and cyclohexane were formed via the disproportionation of cyclohexene formed as a result of dehydration of cyclohexanol[113]. It was reported[114] that cyclohexanone undergoes further transformation to phenol at high contact times. Costa *et al.*[115], by means of deuterium labeling experiments, have shown that the gas phase dehydration of cyclohexanol over a solid zirconium phosphate catalyst, involves a long lived carbocation intermediate and that the reaction proceeds via the E1 mechanistic route.

3.4. CONCLUSIONS

The following conclusions can be drawn from the different physico chemical characterization techniques as well as acidity determination of the sulfated titania systems.

- Nanocrystalline materials of crystallite size upto 5 nm can be easily prepared by this sol-gel method. Anatase is found to be the major phase in all the samples as apparent from XRD data. Sulfate ions hinder the crystallization of titania particles by preventing the agglomerization of surface particles. Sulfation retards the transformation of anatase to rutile.
- Surface area and pore volume of sulfated samples are higher than that of pure titania. The metal oxide species along with the sulfate ions prevent the agglomeration of titania particles resulting in a higher surface area.
- EDX results prove that sol-gel method is an efficient method to prepare supported systems with desired loading of transition metals. The presence of transition metal oxides stabilizes the sulfate over layers on the catalyst surface is apparent from the increase in the sulfate retaining capacity, which is evident from EDX results. SEM pictures clearly give the surface morphology of these catalysts.

- TG/DTG analysis of the catalysts reveals the higher thermal stability of metal incorporated sulfated titania systems even after 700°C. Sulfate incorporation is confirmed by FTIR analysis. λ_{max} and hence band gap energy is calculated from UV-Vis DR spectra, which again confirms the anatase phase of these catalysts. ^1H NMR studies give an idea about the titanol groups present in the catalysis.
- Acidities of the systems are measured by different techniques like NH_3-TPD, perylene adsorption and thermodesorption of 2,6-DMP. Among the different systems 6% metal loaded samples shows the maximum acidity. Cumene conversion reaction proved to be a satisfactory test reaction for surface acidity. The percentage conversion could be correlated with the total acidity of the systems, while the dehydrogenation and cracking selectivity followed trends in the Lewis and Brönsted acidity of the samples respectively. Cyclohexanol decomposition reveals the acid base properties of the prepared catalysts.

REFERENCES

1. A.V. Ramaswamy, "*Catalysis Principles and applications*", Narora, New Delhi.
2. Z. Gao, J.M. Chen, *Chem. J. Chin. Uni.*, 15 (1994) 873.
3. X. Song, A. Sayari, *Catal. Rev. Sci. Eng.*, 38 (1996) 329.
4. G. Colon, M.C. Hidalgo, J.A. Navio, *Appl. Catal.*, 231 (2002) 185.
5. S.K. Samantaray, T. Mishra, K.M. Parida, *J. Mol. Catal. A. Chem.*, 156 (2000) 267.
6. M.M. Dubinin, *Chem. Rev.*, 60 (1960) 235.
7. M.P. Rosynek, P.T. Magnuson, *J. Catal.*, 46 (1977) 402.

8. H. Lipson, H. Steeple, "*Interpretation of X-ray powder Diffraction Patterns*", Macmillan, London, (1970) 261.
9. K. Kandori, S. Uchida, S. Kataoka, T. Ishikawa, *J. Mater. Sci.*, 27 (1992) 719.
10. K.M. Parida, M. Acharya, S.K. Samantaray, T. Mishra, *J. Colloid Interface Sci.*, 217 (1999) 388.
11. D.G. Barton, S.L. Soled, G.D. Meitzner, G.A. Fuentes, E. Iglesia, *J. Catal.*, 181 (1999) 57.
12. L.J. Alemany, M.A. Larrubia, M.C. Jimenez, F. Delgado, J.M. Blasco, *React. Kinet. Catal. Lett.*, 60 (1997) 41.
13. K.R. Sunajadevi, S. Sugunan, *React. Kinet. Catal. Lett.*, 82 (2004) 11.
14. S.T. Choo, Y.G. Lee, I.S. Nam, S.W. Ham, J.B. Lee, *Appl. Catal. A. Gen.*, 200 (2000) 177.
15. A. Corma, *Chem. Rev.*, 95 (1995) 559.
16. Z. Ma, Y. Yue, X. Deng, Z. Gao., *J. Mol. Catal. A. Chem.*, 178 (2002) 97.
17. A.K. Dalai, R. Sethuraman, S.P.R. Katikeneni, R.O. Idem, *Ind. Eng. Chem. Res.*, 37 (1998) 3869.
18. B.I.I. Davis, R.A. Kcogh, R. Sreenivasan, *Catal. Toady*, 20 (1994) 219.
19. J.F. Le Page, J. Cosyns, P. Courty, E. Freund, J.P. Franck, Y. Jacquin, B. Juguin, C. Marcilly, G. Martino, J. Miquel, R. Montarnal, A. Sugier, H. Van Landeghem, "*Applied Heterogeneous Catalysis*", Editions Technip, Paris, (1987) p. 92.
20. C.G. Granqvist, R.A. Buhraman, *J. Appl. Phys.*, 47 (1996) 2200.
21. J. Livage, K. Doi, C. Maziieres, *J. Phys. Chem.*, 93 (1989) 6769.
22. R. Srinivasan, R.A. Keogh, D.R. Milburn, B.H. Davis, *J. Catal.*, 153 (1995) 23.
23. R.A. Keogh, R. Srinivasan, B.H. Davis, *J. Catal.*, 153 (1995) 23.
24. O. Saur, M. Bensitel, A.B.M. Saad, J.C. Lavalley, C.P. Tripp, B.A. Morrow, *J. Catal.*, 99 (1986) 104.

25. H.P. Bochnm, H. Knozinger, "*Catalysis*", J.R. Anderson and M. Boudart, Eds. Vol. 4, Springer, Berlin (1983) Chp. 2.
26. G. Cristallo, E. Roncari, A. Rinaldo, F. Trifiro, *Appl. Catal. A. Gen.*, 209 (2001) 249.
27. J.M. Gallardo-Amores, T. Armaroli, G. Ramis, E. Finocchino, G. Busca, *Appl. Catal. B. Environ.*, 22 (1999) 249.
28. T. Lopez, J.A. Moreno, R. Gomez,X. Bokhimi, J.A. Wang, H. Y. Madeira, G. Pecchi, P. Reyes, *J. Mater. Chem.*, 12 (2002) 714.
29. Y. Su, M.L. Balmer, B.C. Bunker, *J. Phys. Chem. B.*, 104 (2000) 8160.
30. G.D. Yadav, J.J. Nair, *Micropor. Mesopor. Mater.*, 33 (1999) 1.
31. S.M. Jung, O. Dupont, P. Grange, *Appl. Catal. A. Gen.*, 208 (2001) 393.
32. C. Morterra, V. Bolis, G. Cerrato, *Catal. Today*, 17 (1993) 505.
33. A. Clearfield, G.P.D. Serrette, A.H. Khazi-Syed, *Catal. Today*, 20 (1994) 295.
34. L.M. Kustov, V.B. Kazansky, F. Figueras, D. Tichit, *J. Catal.*, 150 (1994) 143.
35. K. Nakamoto, "*Infrared and Raman Spectra of Inorganic and Coordination Compounds*", 4th edition, Wiley, New York (1986).
36. M. Bensitel. O. Saur, J.C. Lavalley, B.A. Morrow, *Mater. Chem. Phys.*, 19 (1988) 147.
37. C. Morterra, G. Cerrato, C. Emanuel, V. Bolis, *J. Catal.*, 142 (1993) 349.
38. M.T. Tran, N.S. Gnep, G. Szabo, M. Guisner, *Appl. Catal.*, 171 (1998) 207.
39. M. Anpo, T. Shima, S. Kodama, Y. Kubokawa, *J. Phys. Chem.*, 91 (1987) 4305.
40. Q. Zhang, L. Gao, J. Guo, *Appl. Catal. B. Environ.*, 26 (2000) 207.
41. Degussa Canada Ltd., Bull. 56, Burlington, Ont., Canada.
42. M.A. Malathi, W.K. Wong, *Surf. Technol.*, 22 (1984) 305.
43. W.K. Wong, M.A. Malathi, *Solar Energy*, 36 (1986) 163.
44. S. Velu, N. Shah, T.M. Jyothi, S. Sivasanker, *Micropor. Mesopor. Mater.*, 33 (1998) 61.

45. F. Milella, j.M. Gallardo-Amores, M. Baldi, G. Busca, *J. Mater. Chem.*, 8 (1998) 2525.

46. G. Ertl, H. Knozinger, J. Weitkamp, "*Handbook of Heterogeneous Catalysis*", (Ed. G. Ertl, H. Knozinger, J. Weitkamp), Vol. I (Wiley VCH), (1997), p. 324.

47. M. Stoker, *Stud. Surf. Sci. Catal.*, 85 (1994) 429.

48. H. Pfeifer, D. Freude, M. Hunger, *Zeolites*, 5 (1985) 274.

49. P.A. Jacobs, W.J. Mortier, *Zeolites*, 2 (1982) 226.

50. M. Weihe, M. Hunger, M. Breuninger, H.G. Karge, J. Weitkamp, *J. Catal.*, 198 (2001) 299.

51. M. Hunger, Catal. *Rev. Sci. Eng.*, 39 (1997) 345.

52. M.A. Enriquez, C. Doremieux-Morin, J. Fraissard, NATO, *Adv. Study Inst. Ser., Ser. C.*, 61 (1980) 409.

53. B.M. Reddy, E.P. Reddy, S.T. Srinivas, V.M. Mastikhin, A.V. Nosov, O.B. Lapina, *J. Phys. Chem.*, 96 (1992) 7076.

54. K.V.R. Chary, V. Vijayakumar, P. Kanta Rao, A.V. Nosov, V.M. Mastikhin, *J. Mol. Catal.*, 96 (1994) L5.

55. L.G. Pinaeva, O.B. Lapina, V.M. Mastikhin, A.V. Nosov B.S. Balzhinimaev, *J. Mol. Catal.*, 88 (1994) 311.

56. V.M. Mastikhin, A.V. Nosov, *React. Kinet. Catal. Lett.*, 46 (1992) 123.

57. M. Crocker, R.H.M. Herold, A.E. Wilson, M. Mackay, C.A. Emeis, A.M. Hoogendoorn, *J. Chem. Soc. Faraday Trans.*, 92(15) (1996) 2791.

58. S. Khabtov, T. Chevreau, J. C. Lavelley, *Micropor. Mater.*, 3 (1994) 133.

59. James E. Huheey, Ellen A. Keiter, ichard L. Keiter, "*Inorganic Chemistry Principles of Structure and Reactivity*" 4th Edn. Published by Pearson Education (Singapore) (2004).

60. B.A. Morrow, R.A. McFarlane, M. Lion, J.C. Lavalley, *J.Catal.*, 107 (1987) 232.

61. J.R. Sohn, H.T. Jang, *J. Catal.*, 136 (1992) 267.

62. J.P. Chen, R.T. Yang, *J. Catal.*, 139 (1993) 277.

63. D. Fraenkel, *Ind. Eng. Chem. Res.*, 36 (1997) 52.

64. S.B. Sharma, B.L. Meyers, D.T. Chen, J. Miller, J. Dumesic, *Appl. Catal. A. Gen.*, 102 (1993) 253.

65. H. Karge, V. Dondur, *J. Phys. Chem.*, 94 (1990) 765.

66. A. Auroux, A. Gervasini, *J. Phys. Chem.*, 94 (1990) 6371.

67. J. LeBars, A. Auroux, *J. Therm. Anal.*, 40 (1993) 1277.

68. D.J. Parrillo, R.J. Gorte, W.E. Farneth, *J. Am. Chem. Soc.*, 115 (1993) 12441.

69. P. Berteau, B. Delmon, *Catal. Today*, 5 (1989) 121.

70. C.H. Lin, S.D. Lin, Y.H. Yang, T. P. Lin, *Catal. Lett.*, 73 (2001) 121.

71. R.J. Gillespie, E.A. Ribinson, *Can. J. Chem.*, 41 (1963) 2074.

72. T. Yamauchi, T. Jin, K. Tanabe, *J. Phys. Chem.*, 90 (1986) 3148.

73. S.M. Jung, P. Grange, *Appl. Catal. A. Gen.*, 228 (2002) 65.

74. S.M. Jung, P. Grange, *Catal. Today*, 59 (2000) 305.

75. J.J. Rooney, R.C. Pink, *Proc. Chem. Soc.*, (1961) 70.

76. B.D. Flockart, J.A.N. Scott, R.C. Pink, *Trans.Farad. Soc.*, 62 (1966) 730.

77. J. Kijenski, A. Baiker, *Catal. Today*, 5 (1989) 1.

78. F. Arena, R. Dario, A. Parmaliana, *Appl. Catal. A. Gen.*, 170 (1998) 127.

79. T. Yamaguchi, *Appl. Catal.*, 61 (1990) 1.

80. A. Corma, V. Fornes, M.I. Juan Rajadell, J.M. Lopez Nieto, *Appl. Catal. A. Gen.*, 116 (1994) 151.

81. R.T. Sanderson, "*Chemical Bonds and Bond Energy*", Academic Press, NewYork (1976) p.75.

82. A. Corma, C. Rodellas, V. Fornes, *J. Catal.*, 88 (1984) 374.

83. A. Satsuma, Y. Kamiya, Y. Westi, T. Hattori, *Appl. Catal. A. Gen.*, 194-195 (2000) 253.

84. J.T. Richardson, *J. Catal.*, 9 (1967) 182.

85. S. Zenon, *Appl. Catal. A.*, 159 (1997) 147.

86. P. Wu, T. Komatsu, T. Yashima, *Micropor. Mesopor. Mater.*, 22 (1998) 343.

87. M.S. Rana, S.K. Maity, J. Ancheyta, G. Murali Dhar, T.S.R. Prasada Rao, *Appl. Catal. A. Gen.*, (2003) in press.

88. P.M. Boorman, R.A. Kydd, Z. Sarbak, A. Somogyvari, *J. Catal.*, 100 (1986) 287.

89. P.M. Boorman, R.A. Kydd, Z. Sarbak, A. Somogyvari, *J. Catal.*, 96 (1985) 115.

90. Narayanan, K. Deshpande, *Appl. Catal. A. Gen.*, 199 (2000) 1.

91. A. Corma, B.W. Wojciechowski, *Catal. Rev. Sci. Eng.*, 24 (1982) 1.

92. J.W. Ward, *J. Catal.*, 9 (1967) 225.

93. W. Przystajko, R. Fieddorow, I.G. Dalla Lana, *Appl. Catal.*, 15 (1985) 265.

94. H.Pines, "*The chemistry of catalytic hydrocarbon conversions*", Academic Press, New York (1981) p.85.

95. A. Corma, J.L.G. Fiero, R. Montanana, F. Tomas, *J. Mol. Catal.*, 30 (1985) 361.

96. F.M. Bautista, J.M. Campelo, A. Garcia, D. Leina, J.M. Marinas, A.A. Romero, *Appl. Catal.*, 104 (1993) 109.

97. F.M. Bautista, J.M. Campelo, A. Garcia, D. Luna, J.M. Marinas, A.A. Romero, J.A. Navio, M. Macias, *J. Catal.*, 145 (1994) 107.

98. S.J. Kulkarni, R. Ramachandra Rao, M. Subrahmanyam, A.V. Rama Rao, *J. Chem. Soc. Chem. Commun.*, (1994) 273.

99. A. Gervasini, A. Auroux, *J. Catal.*, 131 (1991) 190.

100. M.A. Armindia, V. Borau, I.M. Garcia, C. Jimenez, A. Marinas, J.M. Marinas, A. Porras, F.J. Urbano, *Appl. Catal.*, 184 (1999) 115.

101. M.C.C.C. Costa, L.F. Hodson, R.A.W. Johnstone, J.Y. Liu, D. Whitaker, *J. Mol. Catal.*, 142 (1999) 349.

102. D. Martin, Duprez, *J. Mol. Catal.*, 118 (1997) 113.

103. M. Ai, *J. Catal.*, 40 (1975) 318.

104. M. Ai, *Bull. Chem. Soc. Jpn.*, 50 (1977) 2587.

105. C.G. Ramankutty, S. Sugunan, Bejoy Thomas, *J. Mol. Catal. A. Chem.*, 187 (2002) 105.

106. K.V.V.S.B.S.R. Murthy, B. Srinivas, S.J. Kulkarni, M. Subramanyan, P. Kanta Rao, *"Catalysis:Modern Trends"*, N.M.Gupta, D.K.Chakrabarthy (Eds), Narosa Publishing House, New Delhi, (1995) 189.

107. A. Auroux, A. Gervasini, *J. Phys. Chem.*, 94 (1990) 6371.

108. C.P. Bezouhanova, M.A. Al-Zihari, *Catal. Lett.*, 11 (1991) 245.

109. O.V. Krylov, *"Catalysis by Non- metals"*, Academic press, New York (1970).

110. J. Navarette, T. Lopez, R. Gomez, *Langmuir.*, 12 (1996) 4385.

111. L. Nodek, J. Sedlacek, *J. Catal.*, 40 (1975) 34.

112. M. Bowker, R.W. Petits, K.C. Waugh, *J. Catal.*, 99 (1986) 53.

113. M. Dobrovosky, P. Tenyi, Z. Paal, *J. Catal.*, 74 (1982) 31.

114. N.J. Jebaratjoma, V. Krishnaswamy, *"Catalysis: Present and Futures"* (P. Kanta Rao and B.S. Benwal (Edn.)) Publication and information Directorate, New Delhi, p. 288.

115. M.C.C. Costa, L.F. Hudson, R.A.W. Johnstone, J.Y. Liu, D. Whittaker, *J. Mol. Catal.*, 142 (1999) 349.